

# Two functionally distinct Purkinje cell populations implement an internal model within a single olivo-cerebellar loop

Dora E. Angelaki<sup>1</sup>, Jean Laurens<sup>2</sup>

<sup>1</sup> Center for Neural Science and Tandon School of Engineering, New York University, NY, USA.

<sup>2</sup> Ernst Strüngmann Institute (ESI) for Neuroscience in Cooperation with Max Planck Society, Frankfurt, Germany

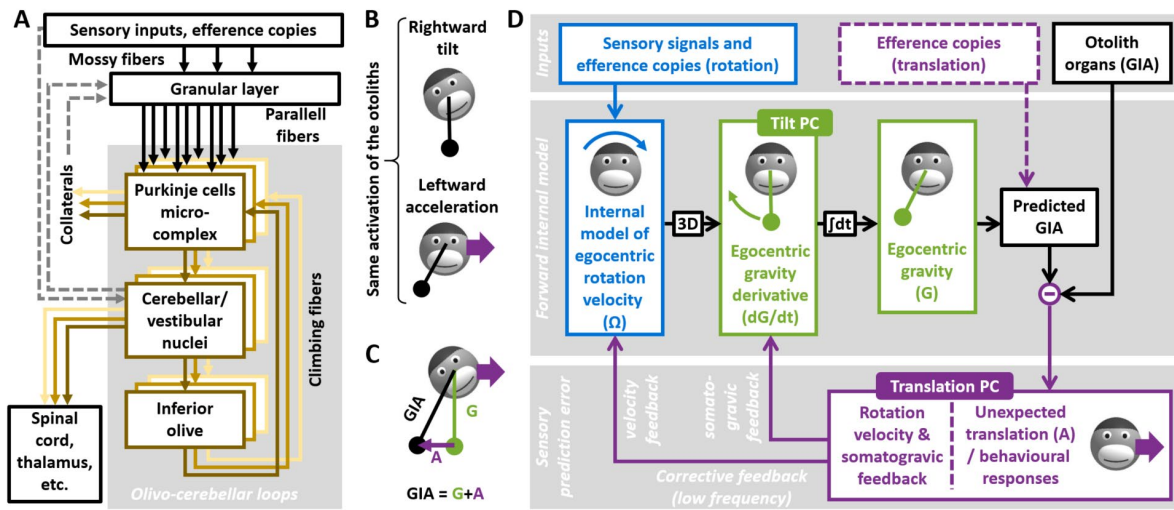
## Abstract

Olivo-cerebellar loops, where anatomical patches of the cerebellar cortex and inferior olive project one onto the other, form an anatomical unit of cerebellar computation. Here, we investigated how successive computational steps map onto olivo-cerebellar loops. Lobules IX-X of the cerebellar vermis, i.e. the nodulus and uvula, implement an internal model of the inner ear's graviceptor, the otolith organs. We have previously identified two populations of Purkinje cells that participate in this computation: Tilt-selective cells transform egocentric rotation signals into allocentric tilt velocity signals, to track head motion relative to gravity, and translation-selective cells encode otolith prediction error. Here we show that, despite very distinct simple spike response properties, both types of Purkinje cells emit complex spikes that are proportional to sensory prediction error. This indicates that both cell populations comprise a single olivo-cerebellar loop, in which only translation-selective cells project to the inferior olive. We propose a neural network model where sensory prediction errors computed by translation-selective cells are used as a teaching signal for both populations, and demonstrate that this network can learn to implement an internal model of the otoliths.

## Introduction

Theories developed over the last decades (Ito, 2006; Kawato, 1999; Wolpert et al., 1998a, 1998b) have proposed that the cerebellum implements forward internal models that predict sensory inflow based on internal representations of the world and our body. Sensory predictions are then compared to actual sensory afference. In the event of mismatches, the resulting sensory prediction errors drive corrective feedback mechanisms to update internal representations and guide perception and action. On a longer time scale, these errors drive learning mechanisms to acquire or calibrate the internal models (Herzfeld et al., 2018; Kimpo et al., 2014; Lisberger, 1988; Nguyen-Vu et al., 2013).

31



32

33 **Figure 1: Olivocerebellar loops, and internal model computations for processing otolith signals. A:**  
 34 *Neural pathways and information processing in olivocerebellar loops. Sensory inputs and efference*  
 35 *copies reach the cerebellum through mossy fibers and are processed in the granular layer. Granule cells*  
 36 *convey this information to PCs through parallel fibers. PCs are anatomically clustered in microzones,*  
 37 *and several microzones participating to a single olivocerebellar loop form a microcomplex. Further*  
 38 *pathways exist in the vestibular circuitry: primary afferents also reach the vestibular nuclei, which*  
 39 *project to the granular layer, and PCs may project collaterals to the granular layer. B: Ambiguity of the*  
 40 *otolith organs. The otolith organs are analogous to a pendulum, whose position is sensed in egocentric*  
 41 *head coordinates. Rightward head tilt or leftward acceleration cause a rightward deviation of the*  
 42 *pendulum relative to the head, resulting in an identical activation of the otoliths. C: Mathematical*  
 43 *formulation of the ambiguity. The otoliths sense the gravito-inertial acceleration (GIA), expressed as*  
 44  *$GIA = G + A$  where  $G$  is the gravity vector and  $A$  a vector opposite to the linear acceleration (this*  
 45 *convention is chosen for clarity purposes). The brain may resolve the ambiguity by tracking  $G$ , and*  
 46 *computing  $A$  by subtraction ( $A = GIA - G$ ). D: Internal model computations for otolith information*  
 47 *processing. See text for description.*

48 Cerebellar computations are implemented by olivocerebellar loops (Fig. 1A) (Apps et al., 2018; Apps  
 49 & Garwicz, 2005; Chaumont et al., 2013; De Zeeuw et al., 2011; Ozden et al., 2009; Sugihara & Quy,  
 50 2007), within which a group of Purkinje Cells (PCs) in the cerebellar cortex project simple spikes (SS)  
 51 to a group of cells in the cerebellum's output nuclei (the deep cerebellar nuclei, DCN, and vestibular  
 52 nuclei, VN). These nuclei project throughout the nervous system to control behaviour, and to a group  
 53 of Inferior Olive (IO) neurons that projects back to the cerebellar cortex. IO neuron influence on PCs  
 54 induces Complex Spikes (CS) that act as teaching signals to drive cerebellar learning (Herzfeld et al.,

55 2018; Kimpo et al., 2014; Lisberger, 1988; Nguyen-Vu et al., 2013). PCs within an olivo-cerebellar loop  
56 are anatomically clustered in sagittally oriented microzones of several hundred microns in length and  
57 tenths of microns in width (Kostadinov et al., 2019; Ozden et al., 2009; Valera et al., 2016). An olivo-  
58 cerebellar loop can be formed by multiple microzones that receive similar projections from the IO,  
59 and collectively form a multizonal microcomplex (Apps & Garwicz, 2005; Cerminara et al., 2020) : in  
60 this study we will use the term 'microcomplex' to refer to a set of PCs receiving identical IO projections,  
61 and 'loop' to refer to the network of cortical, nuclear and IO neurons communicating with a  
62 microcomplex.

63 Studies to date have pioneered the 'microcomplex' as a fundamental unit of cerebellar computation,  
64 e.g. during saccadic eye movements (Herzfeld et al., 2015, 2018), tactile reflexes (Apps & Garwicz,  
65 2005; Cerminara et al., 2020; Ekerot et al., 1991; Garwicz et al., 1998) or cognitive tasks (Kostadinov  
66 et al., 2019). This has led to the notion that identifying PCs that receive identical IO inputs (i.e.  
67 participate in the same microcomplex) allows parsing the cerebellar cortex into elementary  
68 computation units (Herzfeld et al., 2015, 2018; Shadmehr, 2020). However, how to map such multi-  
69 variable computations onto olivo-cerebellar loops raises fundamental questions. One possibility is that  
70 each variable is represented by a different microcomplex such that multivariable computations are  
71 implemented by parallel loops, each computing one variable. Alternatively, it is also possible that PCs  
72 encoding fundamentally distinct variables may exist in a single microcomplex. Such a finding would  
73 depart from the traditional view where one loop computes one variable and suggest that individual  
74 microcomplexes can perform sequences of operations: Functionally distinct PCs perform distinct  
75 computations using common teaching signals.

76 To distinguish between these two hypotheses we take advantage of a multivariable cerebellar  
77 computation based on an internal model of self-motion, already widely studied in the literature (**Fig.**  
78 **1B-D**) (Borah et al., 1988; Bos & Bles, 2002; Glasauer & Merfeld, 1997; Karmali & Merfeld, 2012;  
79 Laurens & Angelaki, 2011, 2017; Laurens & Droulez, 2007; Merfeld, 1995; Oman, 1982; Ormsby &  
80 Young, 1977; Zupan et al., 2002). A unique advantage of this system is the ability to map complex, but  
81 well-understood, algorithmic computations implementing an internal model of the inner ear's inertial  
82 motion sensors, the otolith organs, into a cerebellar circuit that includes lobules X and IX of the  
83 cerebellar vermis (Nodulus and Uvula; NU) (Laurens et al., 2013a, 2013b; Laurens & Angelaki, 2020;  
84 Stay et al., 2019; Yakusheva et al., 2007, 2008, 2013).

85 Specifically, the otolith organs sense the sum of gravitational (G) and linear accelerations (A), which  
86 are physically indistinguishable (Einstein, 1907), in head coordinates (**Fig. 1 B,C**). The otolithic signal is  
87 therefore inherently ambiguous. Nevertheless, this ambiguity can be resolved by using additional

88 sensory information and motor inference copies to predict the two components of otolith activation,  
89 gravity (G) and translational acceleration (A). On the one hand, the gravitational component G can be  
90 predicted by tracking head rotation relative to gravity (**Fig. 1D**, green). A portion of the head's internal  
91 model of motion (**Fig. 1D**, blue; not developed here for simplicity; (see (Karmali & Merfeld, 2012;  
92 Laurens & Angelaki, 2011, 2017) for details), senses head rotation velocity ( $\Omega$ ) in an egocentric frame  
93 of reference. The internal model converts  $\Omega$  into allocentric velocity relative to gravity (block marked  
94 '3D' in **Fig. 1D**), which is equivalent to the derivative of gravity in head coordinates ( $dG/dt$ ). This signal  
95 is integrated over time (block marked 'f' in **Fig. 1D**) to estimate the gravity vector in head coordinates  
96 (G). On the other hand, head translation may be derived directly from motor efference copies during  
97 active translation (**Fig. 1D**, violet, broken lines), but is unpredictable during passive movements.

98 Altogether, the internal model can predict otolith signals during active tilt and translations (based on  
99 motor commands), or during passive tilt (based on rotation signals). Thus, otolith prediction errors  
100 occur during passive translations, or if tilt signals are erroneous, which can occur because of sensory  
101 noise or incorrect rotation signals from the canals. Since these tilt errors are generally smaller and  
102 scarcer, the brain preferentially interprets otolith prediction errors as translation. Accordingly, otolith  
103 prediction errors induce a perception of translation and the corresponding stabilizing eye movements,  
104 irrespective of whether the prediction error originates from an actual translation or an artificially  
105 generated incorrect canal signal (Angelaki et al., 1999; Hess & Angelaki, 1999; Khosravi-Hashemi et al.,  
106 2019; Merfeld et al., 1999). Otolith prediction errors also trigger low-frequency feedback (**Fig 1D**,  
107 violet) that gradually correct the underlying rotation signals and tilt estimates.

108 Based on SS responses exclusively, two populations of PCs were identified that perform distinct steps  
109 in the internal model's computation. First, translation-selective cells (**Fig. 1Ds**) encode otolith  
110 predictions error (Laurens et al., 2013a, 2013b; Laurens & Angelaki, 2020; Stay et al., 2019; Yakusheva  
111 et al., 2007, 2008, 2013). These cells respond selectively to passive translation, indicating that they (i)  
112 receive otolith inputs, (ii) are cancelled by tilt signals originating from rotation sensing (**Fig. 1D**;  
113 Laurens et al., 2013b) and (iii) encode sensory prediction errors that result from artificial canal  
114 stimulation (Laurens et al., 2013a). Critically, the responses of translation-selective cells in the VN and  
115 DCN are attenuated during active head translations (Carriot et al., 2013; Mackrous et al., 2019), a  
116 finding that confirms that the internal model uses efference copies to predict otolith signals.

117 Second, another PC type in the NU encodes tilt velocity (**Fig. 1D**, tilt-selective cells; (Hernández et al.,  
118 2020; Laurens et al., 2013b; Laurens & Angelaki, 2020; Stay et al., 2019)). These cells modulate more  
119 during tilt than translation in phase to tilt velocity (Laurens & Angelaki, 2020). Importantly, 3D motion

120 stimuli have revealed that these cells encode transformed rotation signals ( $dG/dt$ ), and not egocentric  
121 rotation velocity ( $\Omega$ ) (ref).

122 Despite a good understanding on the properties of SS responses, little is currently known about CSs,  
123 which are fundamental for understanding the organisation of the corresponding cerebellar circuits.  
124 Previous CS studies were limited to rotation stimuli (Barmack & Shojaku, 1995; Fushiki & Barmack,  
125 1997; Kitama et al., 2014; Yakhnitsa & Barmack, 2006), or only characterized translation-selective cells  
126 (Yakusheva et al., 2010). A crucial, yet unanswered, question is whether CS firing is different in tilt-  
127 selective and translation-selective cells: this would imply that there are two distinct cerebellar loops.  
128 Alternatively, if tilt-selective and translation-selective cells exhibit similar CS firing, they may comprise  
129 a single loop using the same teaching signals.

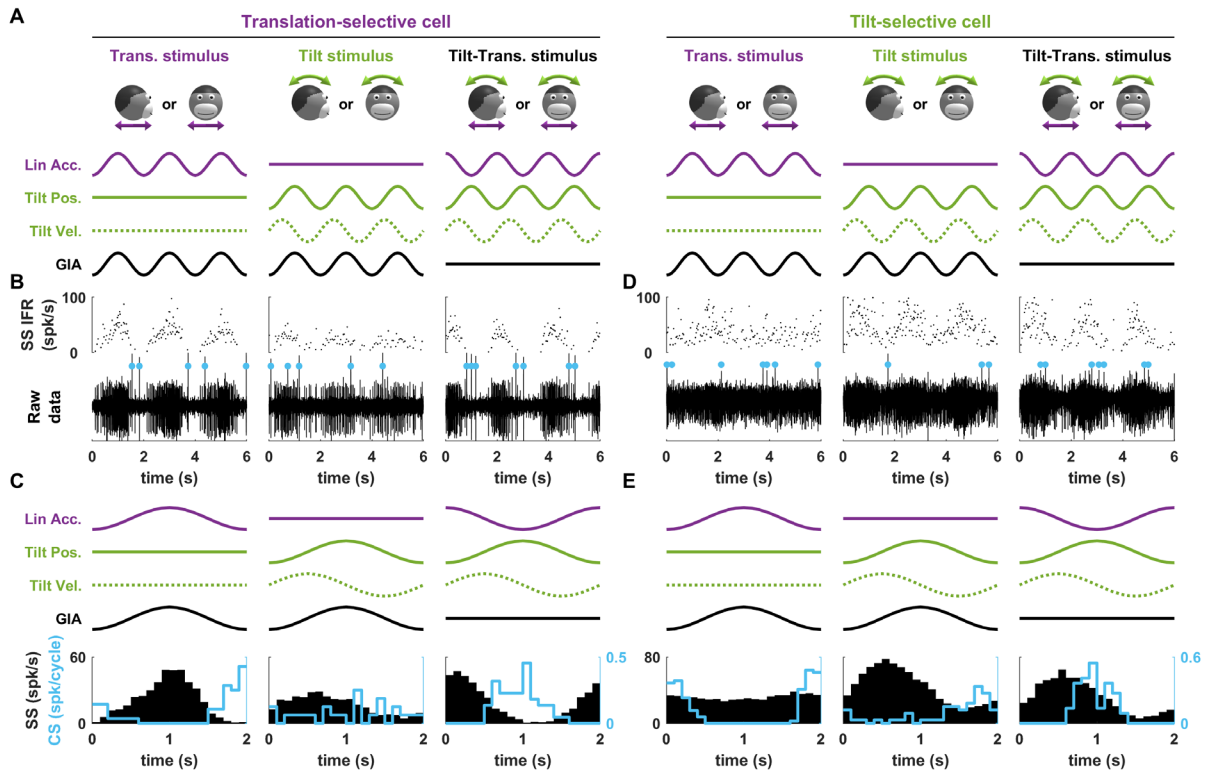
130 Here, we analysed the CS firing of both tilt- and translation-selective cells during combinations of tilt  
131 and translation stimuli, as well as 3D motion (Laurens et al., 2013a, 2013b). Surprisingly, we found  
132 that the CS firing of both cell types is identical, and occurred specifically during translation. This  
133 indicates that the teaching signal to both cell types is driven by otolith prediction error, which is the  
134 output of the internal model implemented by the NU. We interpret these findings in the context of a  
135 previously proposed learning rule (Dean et al., 2002, 2010; Dean & Porrill, 2014), and validate our  
136 interpretation by simulating a neural network model that learns to discriminate tilt from translation.

## 137 **Results**

138 We analysed CSs of 66 out of 211 Purkinje cells recorded in lobules IX-X of the cerebellar vermis  
139 (Laurens et al., 2013a, 2013b) that could be identified consistently across trials and followed by a  
140 pause in SS activity for at least 10 ms. Neurons were recorded during sinusoidal translation (**Fig. 2A**,  
141 left) and tilt (**Fig. 2A**, middle) at 0.5 Hz (Angelaki et al., 1999, 2004; Laurens et al., 2013a, 2013b; Shaikh  
142 et al., 2005; Yakusheva et al., 2007, 2008, 2013), which activated the otoliths identically (**Fig. 2A**, GIA).  
143 A few cells were also recorded during: (1) out-of-phase tilt and translation (tilt-translation, **Fig. 2A**,  
144 right), where linear acceleration and tilt cancel each other, such that the otoliths are not activated but  
145 the canals sense velocity; and (2) in-phase tilt + translation (not represented in figures; see (Laurens  
146 et al., 2013b; Laurens & Angelaki, 2016)). We used a spatio-temporal tuning model (Laurens et al.,  
147 2013b; Laurens & Angelaki, 2016) together with a bootstrap test to classify cells as translation-  
148 selective (larger response to translation), tilt-selective (larger response to tilt), GIA-selective (same  
149 response to tilt and translation, similar to otolith afferents), composite (cells who could not be  
150 classified in one of these categories) or non-responsive.

### 151 *Example cells*

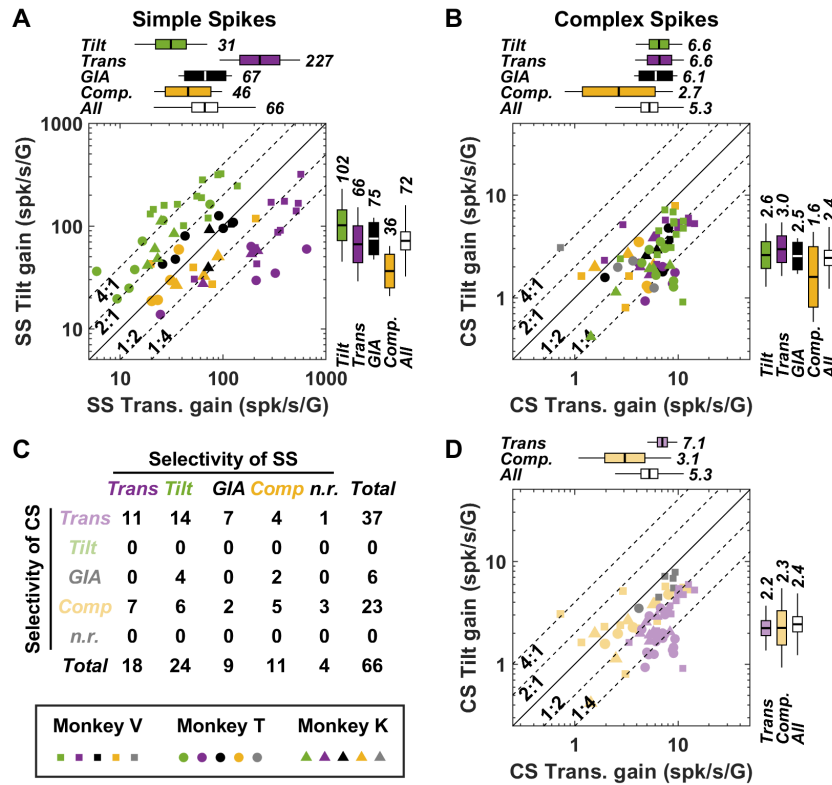
152 Responses of example tilt- and translation-selective neurons are shown in **Fig. 2**. The translation-  
 153 selective cell (**Fig. 2B,C**) shows vigorous SS response during translation (**Fig. 2B,C, left**), but not during  
 154 tilt (**Fig. 2B,C, middle**). During translation, the cell fired CSs during the trough of the SS response (**Fig.**  
 155 **2B,C, left**, marked by cyan dots). In contrast, the phase-locked firing was weaker during tilt (**Fig. 2B,C,**  
 156 **middle**). During tilt-translation (**Fig. 2B,C, right**), SSs and CSs maintained their phase relationship  
 157 relative to the translational component of the stimulus, as expected if they were both driven by  
 158 translation.



159 **Figure 2: Representative Purkinje cells during tilt/translation. A:** illustration of the motion stimuli.  
 160 Violet and solid green curves: inertial acceleration and tilt position; the sum gives the GIA (black). Tilt  
 161 velocity is indicated by broken green curves. **B:** Spiking activity of a translation-selective cell. Bottom  
 162 traces show the raw extracellular voltage. CSs are marked by cyan dots. Upper traces show  
 163 instantaneous firing rate (IFR) of the SSs. **C:** Average firing histograms of SSs (black) and CSs (cyan).  
 164 **D,E:** Spiking activity and average firing of a representative tilt-selective cell (layout as in B,C).

166 The second example neuron (**Fig. 2D,E**) is representative of tilt-selective cells (Laurens et al., 2013b;  
 167 Laurens & Angelaki, 2020; Stay et al., 2019): SS modulation was higher during tilt compared to  
 168 translation (**Fig. 2D,E, middle versus left**). Consistently, groups of 2-3 CSs occurred at regular phases  
 169 during each cycle of translation (**Fig. 2D, left**), such that a clear CS modulation occurred during  
 170 translation (**Fig. 2E, left**). In contrast, CS modulation was weaker during tilt (**Fig. 2E, middle**). During

171 tilt-translation (Fig. 2D,E, right), when SSs occurred during tilt (Fig. 2E, right versus middle), CS  
 172 modulation maintained its phase with respect to the translational component of the stimulus. Thus,  
 173 this cell's CS firing (Fig. 2E) was locked to head translation, and conspicuously similar to that of the  
 174 translation-selective cell (Fig. 2C).



175

176 **Figure 3: Response modulation and classification of the SS and CS firing across the population of PCs.**  
 177 **A:** Tilt versus translation response gain of SS firing. Cells are color-coded based on their classification  
 178 (green, violet, back and yellow: tilt-, translation-, GIA-selective and composite). Marker shapes indicate  
 179 the animal in which cells were recorded (see legend on lower left corner). The boxes and whisker plots  
 180 represent geometrical average (box center), 95% confidence interval (box) and standard deviation  
 181 (whiskers) of the gain for each cell type and all cells together (white). Broken black lines parallel to the  
 182 diagonal represent the level at which tilt response gain is 4x, 2x, 1/2x and 1/4x the translation response  
 183 gain. **B:** Tilt versus translation response gain of CS firing. Cells are color-coded based on their SS  
 184 classification, i.e. as in A. **C:** Contingency matrix between the classification of SS and CS response  
 185 sensitivity. **D:** Tilt versus translation response gain of CS firing, as in B, but with cells classified based  
 186 on their CS response (green, violet, grey and yellow: tilt-, translation-, GIA-selective and composite).

187 SS and CS response gains

188 Consistent with previous studies (Laurens et al., 2013b, 2013b; Laurens & Angelaki, 2020; Stay et al.,  
 189 2019), cells were classified based on their SS response gain to tilt and translation, computed along the

190 preferred direction (PD) and expressed in identical units of spk/s/G. By definition, the gains of 18/62  
191 cells (29%) translation-selective cells appear below the diagonal (**Fig. 3A**, violet) since they respond  
192 more to translation, spanning a range of 100 to 1000 spk/s/G. The gains of 24/62 (39%) tilt-selective  
193 cells appear above the diagonal (**Fig. 3A**, green), spanning 20 to 300 spk/s/G during tilt, but orders of  
194 magnitude smaller during translation. GIA-selective and composite cells (20/62, 32%) lie close to the  
195 diagonal. These proportions and ranges of response gains resemble those reported by the broader  
196 cell population (Laurens et al., 2013b), indicating that the cells analysed here are representative of the  
197 full population. Furthermore, they are similar to the population responses of subsequent studies using  
198 stimuli based on Gaussian (rather than sinusoidal) temporal profiles (Laurens & Angelaki, 2020) or  
199 recorded in mice (Stay et al., 2019).

200 We next examined the modulation gain of CS. In **Fig. 3B**, neurons are color-coded based on the  
201 selectivity of their SS response, i.e. as in **Fig. 3A**. Remarkably, most neurons, including all tilt-selective  
202 cells (green), appeared below the diagonal. Thus, like the examples in **Fig. 2**, the CS modulation of  
203 both translation- and tilt-selective cells was higher during translation than tilt. In fact, the average CS  
204 modulation of tilt-, translation- and GIA-selective cells were identical during translation (6.6, 6.6 and  
205 6.1 spk/s/G respectively, **Fig. 3B**, upper box plots;  $p=0.79$ , Krusal-Wallis non-parametric ANOVA) and  
206 also during tilt (2.6, 3 and 2.5 spk/s/G respectively, **Fig. 3B**, rightward box plots;  $p=0.65$ , Krusal-Wallis  
207 non-parametric ANOVA). CS response gains appeared weaker and more variable in composite cells  
208 (**Fig. 3B**, yellow boxes) and in cells whose SS didn't exhibit a significant modulation (**Fig. 3B**, grey  
209 markers).

210 To evaluate whether CS modulation is significant on a cell-by-cell basis, we used the same classification  
211 method used for SSs. We found that the majority of CS responses (37/66, 56%, **Fig. 3C**) was  
212 independently classified as translation-selective, including most (14/24, 58%) cells that were classified  
213 as tilt-selective based on their SSs. These cells appear in violet in **Fig. 3D**. CS modulation was similar  
214 during tilt and translation in a few cells (6/66, 9%, **Fig. 3C**; grey markers in **Fig. 3D**). In the rest of the  
215 population of cells (23/66, 35%), CS were classified as composite, indicating that they responded to  
216 combinations of tilt and translation (**Fig. 3C**; yellow markers in **Fig. 3D**). Translation responses were  
217 still larger than tilt responses in the majority (18/23) of these cells. Remarkably, no CS response was  
218 classified as tilt-selective. This analysis confirms that CS are generally modulated during translation  
219 and not during tilt, regardless of the selectivity of SS responses.

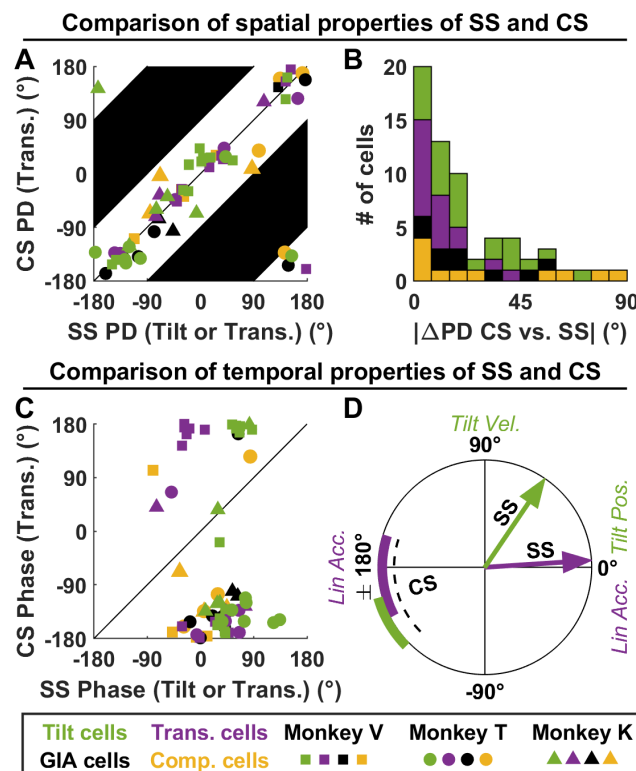
#### 220 Spatio-temporal relationships of SS and CS firing

221 We next investigated whether SS and CS responses are spatially and temporally matched. All cells  
222 were recorded along the forward-backward and lateral directions, allowing us to reconstruct the



223 neuron's tuning curve along all directions (see (Green et al., 2005; Laurens & Angelaki, 2016) for  
 224 details) and determine the direction along which its response is maximal (PD). These PD are  
 225 determined separately for SSs and CSs; and we test whether they are aligned in **Fig. 4A**. Note that SSs  
 226 and CSs may occur along the same axis, but in anti-phase (e.g. as in **Fig. 2C**). In this case, it is equivalent  
 227 to state that they have similar PD and opposite phase, or that they have similar phase and opposite  
 228 PD. We adopt the former convention here: as a consequence, the difference in PD between SSs and  
 229 CSs is never higher than 90°, and the corresponding area is blacked out in **Fig. 4A**. Note also that, since  
 230 CSs are modulated during translation in tilt-selective cells, we compare the PD and phase of SSs during  
 231 tilt to the PD and phase of CSs during translation in tilt-selective cells. For all other cell types, we  
 232 compare SS and CS responses during translation. Note also that PDs are computed relative to the  
 233 direction of the GIA, which is the stimulus activating the otoliths. For instance, a rightward tilt and  
 234 leftward acceleration activate the otoliths in the same manner (**Fig. 1B**) and therefore correspond to  
 235 the same PD.

236



237

238 **Figure 4: Spatio-temporal comparison of SS and CS responses.** **A:** Comparison of the PD of SSs (during  
 239 tilt in tilt-selective cells and translation in other response groups) and CSs (during translation in all  
 240 groups). Note that, by convention, the PD of SS and CS are never more than 90° apart (see text; the  
 241 corresponding areas are marked in black). **B:** Histogram of the PD differences, measured as in A. **C:**  
 242 Comparison of the response phase of SSs (during tilt in tilt-selective cells and translation in other

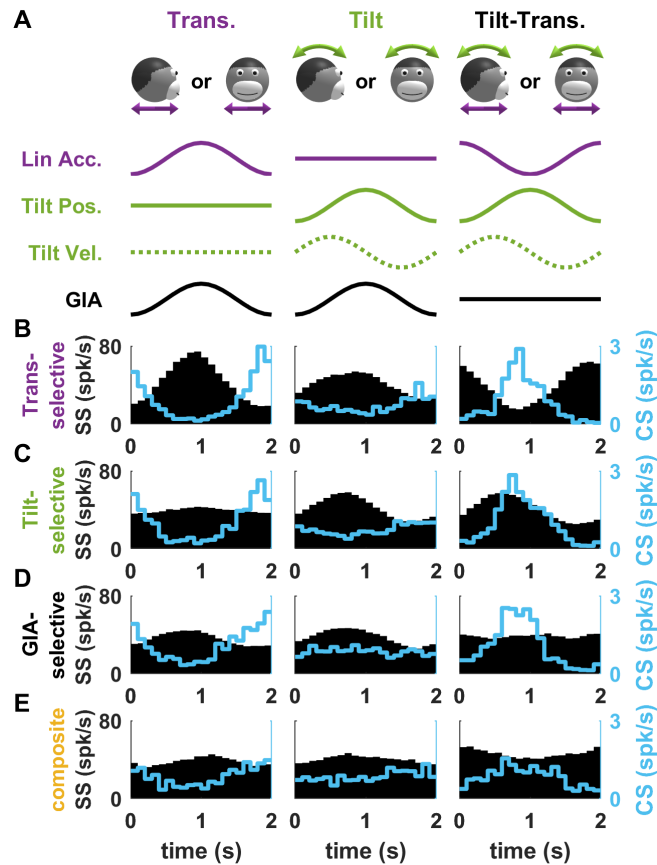
243 *response groups) and CSs (during translation in all groups) during motion along the PD (defined as in*  
244 *A). D: Average response phase of SS (arrow) and CS (sectors representing confidence intervals) in tilt-*  
245 *and translation-selective cells.*

246 We found that the spatial properties of SS and CS were closely aligned. Indeed, their PDs clustered  
247 tightly along the diagonal in **Fig. 4A**. To measure how closely the PDs of SSs and CSs align, we computed  
248 the absolute difference between them (**Fig. 4B**): this difference can range between 0° (when PDs are  
249 aligned) and 90° (when they are orthogonal), and would be distributed uniformly if the PDs of SSs and  
250 CSs were independent. We found that this difference was concentrated close to 0° (**Fig. 4B**; median:  
251 14°, [10 19] CI; Kolmogorov-Smirnov test against uniform distribution:  $p < 10^{-10}$ ), which confirm that the  
252 PDs of SSs and CSs typically align closely.

253 We next examined the response phase of SSs and CSs. In line with our findings in (Laurens et al., 2013b;  
254 Laurens & Angelaki, 2020), the SS response phase of translation-selective cells was close to peak  
255 acceleration (**Fig. 4C**, violet; **Fig. 4D**, violet arrow), and that of tilt-selective cells was close to tilt  
256 velocity (**Fig. 4C**, green; **Fig. 4D**, green arrow). In contrast, we found that the CS response phase during  
257 translation clustered tightly close to -180° in both translation-selective cells (**Fig. 4C,D**; mean: -175°, [-  
258 198 -152] CI) and tilt-selective cells (**Fig. 4C,D**; mean: -154°, [-173 -135] CI). This confirms that the CS  
259 response of the entire population is homogenous in term of response phase, and identical in tilt- and  
260 translation-selective cells.

#### 261 The tilt/translation discrimination microcomplex

262 Previous studies (Herzfeld et al., 2015; Shadmehr, 2020) have proposed that groups of PC within a  
263 microcomplex, i.e. group of PCs that receive similar IO inputs, form a unit of cerebellar computation.  
264 Our results indicate that microcomplexes in the NU are formed by mixtures of tilt-, translation-, GIA-  
265 selective and composite PCs. In the next analysis, we pooled our data to compute of CS and SS  
266 responses of average PCs within a NU microcomplex.

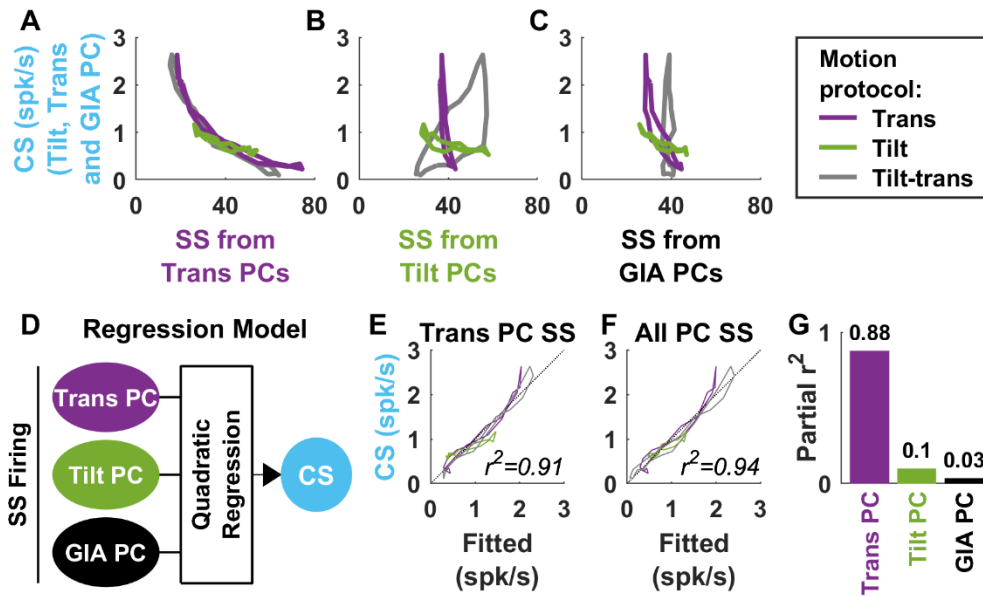


267

268 **Figure 5: Average SS and CS firing histograms of PCs belonging to a common microcomplex. A:**  
 269 *Illustration of the motion stimuli and variables. B-E: Firing histograms of PC belonging to all response*  
 270 *groups. Black histograms: SS firing. Blue histograms: CS firing.*

271

272 To do so, we computed the PD of each cell CS, and computed the SS and CS firing histograms across  
 273 all trials collected within  $\pm 45^\circ$  of the PD. This allowed us to ‘spatially align’ the firing of PCs with various  
 274 PD and to average their CS and SS responses. In agreement with **Fig. 3, 4**, we found that the CS  
 275 response profile of translation-, tilt- and GIA-selective cells are highly similar (**Fig. 5B-D**, cyan).  
 276 Furthermore, the average SS responses of both translation- and tilt-selective cells followed the typical  
 277 pattern of cells in these categories, with translation-selective cells encoding linear acceleration and  
 278 tilt-selective cells encoding tilt velocities. This indicates that, within a microcomplex, translation- and  
 279 tilt-selective PC have homogenous SS responses such that their activity may be pooled to form a  
 280 ‘super-PC’ (Apps et al., 2018). In contrast, the SS response modulation of GIA-selective and composite  
 281 cells was modest, indicating that these groups may not form coherent populations.



282

283 **Figure 5S1: CS firing can be predicted based on SS from translation-selective cells.** A-C: CS response  
 284 (from Fig. 5B-D; averaged across tilt-, translation- and GIA-selective PC) versus SS response of  
 285 translation-selective (A), tilt-selective (B) and GIA-selective PC (from Fig. 5B). There is a clear inverse  
 286 relationship between CS and the SS from translation-selective cells (A). Importantly, this relationship  
 287 holds across all motion protocols, including tilt (green). In contrast, there is no consistent relation  
 288 between the CS and the SS of tilt- and GIA-selective cells. Therefore, it appears that CS firing can be  
 289 predicted based on the SS of translation-selective cells only. D: To test this, and investigate the SS of  
 290 tilt- of GIA-selective cells can make any significant contribution to predicting CS firing, we perform a  
 291 multiple regression analysis where SS are the predictors and CS the dependent variable. We use a  
 292 quadratic regression to account for the curvature of the curves in A. E,F: Relation between fitted  
 293 (abscissae) and measured (ordinate) CS firing when the regression uses the SS of translation-selective  
 294 cells (E) or of all cells (F) as a predictor. The high  $r^2$  score in (E) indicates that SS from translation-  
 295 selective cells explain CS firing accurately, and increases only marginally in (F), indicating and SS from  
 296 other cell types provide little additional information. G: Partial correlation analysis: based on the same  
 297 rationale as panels E-F, each variable's partial  $r^2$  reflects how much adding this variable to the others  
 298 increase the regression's overall  $r^2$ . The partial  $r^2$  of SS from translation-selective PC is high and  
 299 significant ( $p < 10^{-3}$ , shuffling test), whereas the partial  $r^2$  of SS from other cell types is not significantly  
 300 higher than expected by chance ( $p=0.064$  and  $p=0.41$ ). Thus, from a statistical point of view, the SS of  
 301 tilt- and GIA-selective cells don't contribute significantly to predicting CS firing.

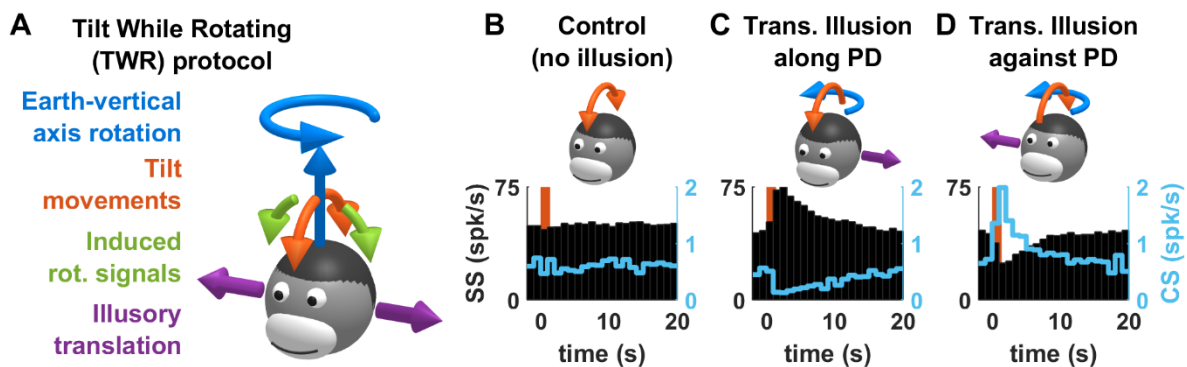
302 In most cell groups (translation-, tilt- and GIA-selective PCs), CSs occur predominantly during  
 303 translation, suggesting that IO regions that innervate the NU are under the control of translation-  
 304 selective PCs. Yet, CSs also exhibited a smaller but visible modulation during tilt. Does it indicate that

305 the same IO regions are also under the control of tilt-selective PC? We note that translation-selective  
 306 cells also modulate to a limited extent during tilt (**Fig. 5B**). Therefore, it is possible that translation-  
 307 selective cells alone control the IO, and are sufficient to account for the modulation of CS during tilt.  
 308 To test this possibility, we conducted a multiple regression analysis between SS and CS firing (**Fig. 5S1**).  
 309 We found that using the SS activity of translation-selective PC predicts CS modulation during both  
 310 translation and tilt, and that adding the SS activity of tilt-selective cells as predictors didn't improve  
 311 the fitting significantly. There is therefore no evidence that tilt-selective cells influence CS firing in the  
 312 NU.

313 Thus, in summary, the data in **Fig. 5** offers a synthetic overview of a cell population which putatively  
 314 constitute a unit of computation in the NU. We will explore the possible architecture of such a circuit  
 315 further using modelling. Before this step, we will examine CS responses during 3D motion protocols  
 316 used in (Laurens et al., 2013a, 2013b).

317

318 Three-dimensional responses and motion illusions



319

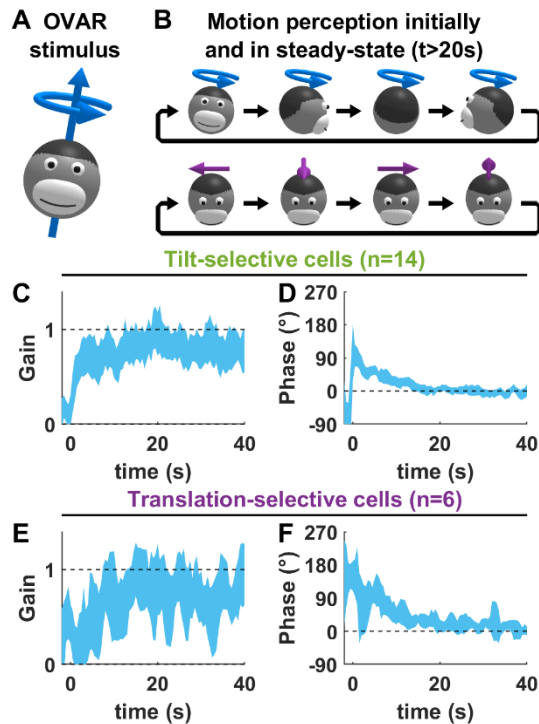
320 **Figure 6: SS and CS responses of translation-selective cells induced by Tilt While Rotating. A:**  
 321 *Rationale of the protocol (see text for details). B-D: SS (black) and CS (cyan) responses during control*  
 322 *tilt (B) or TWR inducing illusory translation along (C) or opposite (D) to the SS PD.*

323 We first analysed CS responses of PCs during Tilt While Rotating (TWR; **Fig. 6**; see (Laurens et al.,  
 324 2013a) for details). TWR consists of alternating tilt (i.e. forward/backward as illustrated in **Fig. 6A**,  
 325 orange, or left/right) movements that are superimposed on a constant-velocity rotation about an  
 326 earth-vertical axis (**Fig. 6A**, blue). Due to the high-pass filter nature of the semicircular canals, TWR  
 327 induces rotation signals in a direction orthogonal to the actual tilt (e.g. roll; **Fig. 6A**, green), even  
 328 though the head doesn't move in this direction. Processing these signals through an internal model  
 329 produces a sensory prediction error which, according to the internal model framework in **Fig. 1D**, leads  
 330 to illusory translation (sideward, **Fig. 6A**, violet). In (Laurens et al., 2013a), we demonstrated that the

331 SS firing of translation-selective PCs increases or decreases when TWR induces illusory translation  
332 along or opposite to their PD.

333 We analysed the CS firing of a subset of these cells in which CS could be reliably identified: this includes  
334 9 translation-selective cells as well as 1 tilt-selective, 3 GIA-selective and 1 composite cell. For  
335 simplicity, only the translation-selective cells are included in **Fig. 6** (because of the limited number of  
336 other cells categories, pooling them with translation-selective cells produces identical results). As  
337 reported previously (Laurens et al., 2013a), PCs were not modulated by a control condition where tilt  
338 movements occurred in the absence of earth-vertical axis rotation (**Fig. 6B**, black) but discharged SSs  
339 when TWR induced illusory translation along their PD (**Fig. 6C**, black) or were inhibited when TWR  
340 induced illusory translation in the opposite direction (**Fig. 6D**, black). The modulation of CSs followed  
341 a reciprocal pattern (**Fig. 6C,D**, cyan), such that CSs increased when TWR induced an illusory  
342 translation opposite to the cell's PD. This observation confirms our hypothesis that CSs are driven by  
343 an internal model of head motion that generates illusory translation signals during TWR (Laurens et  
344 al., 2013a; Merfeld et al., 1999). It also confirms that CSs occur in opposition to SSs, a point which  
345 could not be formally established from sinusoidal stimuli where the opposite phase between SSs and  
346 CSs could conceivably be attributed to a time delay.

347 We next analysed CS responses during Off-Vertical Axis Rotation (OVAR; **Fig. 7**; see (Laurens et al.,  
348 2013b) for details). OVAR consists in tilting the head's vertical axis (**Fig. 7A**, blue) away from vertical  
349 and then rotating at a constant speed about that axis. Accurate tilt perception during OVAR (**Fig. 7B**,  
350 top) thus requires integrating rotation signals about the head's vertical axis. We demonstrated in  
351 (Laurens et al., 2013b) that the SS firing of tilt- and translation-selective cells reflect this tilt perception,  
352 which demonstrated that the internal model outlined in **Fig. 1D** can operate during 3D motion; and  
353 notably that tilt-selective cells integrate 3D rotation signals to compute  $dG/dt$ . Furthermore, due to  
354 the canal's high-pass filter properties, angular velocity signals fade out in  $\sim 20$  s during OVAR. In this  
355 situation, accurate tilt perception is gradually replaced by a translation illusion (Vingerhoets et al.,  
356 2006, 2007) (**Fig. 7B**, bottom). In (Laurens et al., 2013b), we demonstrated that translation-selective  
357 cells encode this illusion.



358

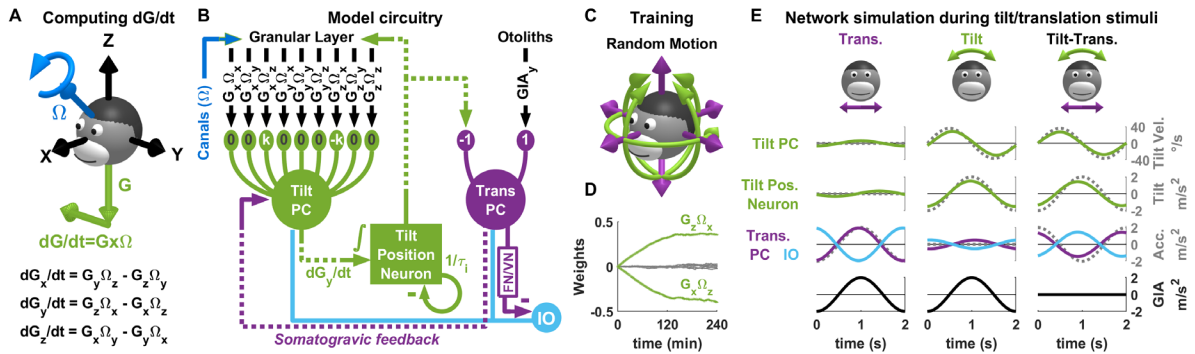
359 **Figure 7: CS responses during OVAR. A,B:** Rationale of the OVAR protocol. The head rotates at a  
 360 constant velocity around a tilted axis. Initially (B, top), the motion is perceived correctly as a dynamic  
 361 tilt stimulus. However, rotation signals from the semicircular canals fade out in about 20 s, resulting in  
 362 a steady-state where OVAR is perceived as a dynamic acceleration stimulus (B, bottom). **C,D:** CS  
 363 response gain and phase of tilt-selective cells, where a gain of 1 and a phase of 0 correspond to the  
 364 response during a translation stimulus equivalent to the steady-state motion (B, bottom). **E,F:** CS  
 365 response gain and phase of translation-selective cells.

366 Since our results indicate that CSs occur during real or illusory translation, we expect that both tilt-  
 367 and translation-selective cells fire CSs during the late stages of OVAR. Furthermore, if CS firing is driven  
 368 by the output of a 3D model of head motion, then CSs should not occur at the beginning of OVAR,  
 369 when integrating 3D rotation cues allows the brain to track head tilt accurately. To test these  
 370 predictions, we analysed CS firing in both tilt-selective cells (n=14) and translation-selective cells (n=6).  
 371 In each population, we computed the CS modulation gain and phase. We found that CS modulation  
 372 was low at the beginning of OVAR and increased until it reached a steady-state in both cell types (**Fig.**  
 373 **7, C,E**). In this steady-state, CS modulation was close to the modulation during translation  
 374 (corresponding to a gain of 1, **Fig. 7, C,E**). Furthermore, the modulation phase evolved from a phase  
 375 lead of  $\sim 90^{\circ}$  (relative to the phase during translation) to a phase of  $0^{\circ}$ , in line with the dynamics of the  
 376 translation illusion during OVAR (see (Laurens et al., 2013b)). These results confirm that CS firing is  
 377 controlled by neurons that implement 3D internal model computations, as outlined in **Fig. 1D**.

378 Neuronal network model

379 The finding both tilt-selective and translation-selective cells receive similar IO inputs raise the  
 380 possibility that they may use the same teaching signal to learn two fundamentally different  
 381 operations. We designed a neural network model (**Fig. 8A,B**) to test whether this process is possible.  
 382 This network reflects the computations outlined in **Fig. 1D**, as described below.

383



384

385 **Figure 8: Neuronal network model of tilt/translation disambiguation.** **A:** Mathematical formulation  
 386 of the transformation performed by tilt-selective cells. Converting egocentric rotation signals ( $\Omega$  blue)  
 387 into tilt-velocity ( $dG/dt$ , green) requires a vectorial cross-product, whose formula is shown at the  
 388 bottom of the panel. **B:** Structure of one olivo-cerebellar loop in the simulated neuron network. This  
 389 loop receives otolith inputs (top right) encoding the lateral component of the GIA, i.e.  $GIA_y$ . During  
 390 learning, the PD of all other cells align with this axis. In the full network, we simulate loops receiving  
 391 otolith inputs along all cardinal axes. These loops operate independently, with one exception: the  
 392 granular layer upstream of tilt PC receives output from tilt position neurons from all loops, which  
 393 provide the gravity signal  $G$  along all dimensions. **C:** The network is trained using random rotations  
 394 and translations in 3D. **D:** Evolution of the synaptic weights of a tilt PC encoding  $dG_y/dt$ . Bands  
 395 represent mean  $\pm$  sd over 15 simulations. Green: synaptic weights of the components required to  
 396 compute  $dG_y/dt$ ; grey: synaptic weights of other components. **F:** Simulated response of all neurons in  
 397 the network during tilt, translation and tilt-translation.

398 Tilt-selective PCs (**Fig. 8B**, 'Tilt PC') compute tilt velocity, i.e. the derivative of gravity  $dG/dt$ .  
 399 Mathematically, tilt velocity can be expressed as the vectorial cross-product  $G \times \Omega$ , which can be  
 400 decomposed into combinations of products (**Fig. 8A**): for instance, lateral tilt velocity,  $dG_y/dt$ , is  
 401 computed as  $G_z\Omega_x - G_x\Omega_z$ . We propose that granule cells encode all 9 possible products ( $G_x\Omega_x$ ,  $G_x\Omega_y$ ,  
 402 etc; **Fig. 8B**), and that tilt-selective PCs learn to combine these products. For instance, to encode  
 403  $dG_y/dt$  (with a gain factor  $k$ ), a tilt-selective cell would associate a weight of  $k$  to  $G_z\Omega_x$ ,  $-k$  to  $G_x\Omega_z$ , and  
 404 0 to all other products. In this respect, our model follows the Marr-Albus hypothesis, in which granule



405 cells act as basis functions (Albus, 1971; Marr, 1969). In (Laurens et al., 2013b; Laurens & Angelaki,  
 406 2020), we noted that, even though tilt-selective PCs primarily encode tilt velocity, their firing is  
 407 partially shifted toward tilt position. To reproduce this property, we modelled these cells as leaky  
 408 integrators with a short time constant of 50ms.

409 The output of tilt-selective PCs is integrated temporally to yield an estimate of tilt position (i.e.  $G$ ) by  
 410 “tilt position neurons” (whose nature is currently unknown) (**Fig. 8B**). Since it is questionable whether  
 411 neurons can perform a perfect integration, we model these neurons as leaky integrators with a time  
 412 constant of 1.2s. Tilt position neurons project to translation-selective PCs, as well as to the granular  
 413 layer in which they provide the gravity signal required to compute  $G \times \Omega$ .

414 Translation-selective PCs (**Fig. 8B**) combine the tilt estimate and the raw otolith signals to compute  
 415 net translation. The polarity of this connection can be deduced as follow: based on **Fig. 5**, we know  
 416 that a translation cell with a given PD (e.g. leftward acceleration), receives the same IO input as a tilt-  
 417 selective cell with an equivalent PD (e.g. rightward tilt velocity, see **Fig. 1B**). Therefore, the pathway  
 418 between tilt-selective and translation-selective PCs should be altogether *inhibitory*. Note, however,  
 419 that the actual pathway between tilt-selective and translation-selective cells involves an unknown  
 420 number of synapses. For clarity, we describe it as an entirely excitatory pathway that terminates with  
 421 a final inhibitory synapse to the translation-selective PC. In practice, the polarity of the individual  
 422 connections may be changed without loss of generality.

423 Translation-selective cells also project to tilt-selective cells (**Fig. 8B**; see also **Fig. 1D**), as shown in  
 424 (Laurens et al., 2013b) to implement a well-known mechanism (Graybiel, 1952) called somatogravic  
 425 feedback (Laurens & Angelaki, 2011, 2017), which prevents the tilt position neurons from  
 426 accumulating errors as they integrate noisy inputs over time and compensates for the leaky dynamics  
 427 of the tilt position neurons.

#### 428 Learning rule

429 Translation-selective PCs project to the IO though an inhibitory pathway. Next, we assume that IO  
 430 signals drive synaptic plasticity according to the following rule (Dean et al., 2002, 2010; Dean & Porrill,  
 431 2014):

$$432 \quad \delta w(t) = l \cdot \text{input}(t) \cdot \text{cs}(t)$$

433 Where  $\text{input}(t)$  and  $\text{cs}(t)$  are the synaptic inputs for a given synapse and the IO inputs, respectively,  
 434  $\delta w(t)$  is the change of synaptic weight, and  $l$  a learning factor. This rule implements a mechanism  
 435 called ‘decorrelation learning’ (Dean et al., 2002, 2010; Dean & Porrill, 2014) through which the circuit  
 436 outlined in **Fig. 8B** learns to cancel its otolith input ( $GIA$ ) based on its canal input ( $\Omega$ ), which amounts

437 to computing a tilt signal. Note that, in this model, this mechanism is more elaborate than in previous  
438 work (Dean et al., 2002, 2010; Dean & Porrill, 2014) since it involves a non-linear operation (the cross-  
439 product  $G_x\Omega$ ) as well as a temporal integration from tilt velocity to position.

440 A priori, synaptic plasticity could occur at all synapses in the network; however, the synaptic weights  
441 between tilt-selective PCs and tilt position neurons, and between tilt position neurons and translation-  
442 selective PCs amount to a simple gain factor, which is redundant with the overall gain of the active  
443 synapses of tilt-selective PCs. Therefore, for simplicity, we only consider plasticity at the level of tilt-  
444 selective PCs.

#### 445 Spatial tuning

446 A notable feature of this model is that the spatial selectivity of tilt-selective PCs and tilt position  
447 neurons is not fixed a priori, since synaptic weights are initialized randomly. Instead, their spatial  
448 selectivity is acquired through learning. In the example of **Fig. 8B**, the otolithic input to the translation  
449 PC encodes lateral GIA ( $GIA_y$ ), and other cells acquire the same spatial selectivity during learning. In  
450 order to create a full 3D model, we simulated 3 parallel loops that process  $GIA_x$ ,  $GIA_y$  and  $GIA_z$ . The tilt  
451 position neurons in these 3 loops provide the components  $G_x$ ,  $G_y$ ,  $G_z$  required to compute  $G_x\Omega$ .

#### 452 Simulation

453 We trained the model during simulated 3D motion (**Fig. 8C,D**), and then simulated all cell types during  
454 tilt and translation stimuli identical to those used in the experiments. For simplicity, we show the  
455 responses of the circuit in **Fig. 8B**, that encodes lateral motion. Since the training procedure uses  
456 uniform 3D motion, the response of the other circuits to comparable stimuli would be identical.

457 The synaptic weights of the tilt-selective PC were initialized randomly (following a Gaussian  
458 distribution with a standard deviation of 0.2) priori to training. During training, the weights  
459 corresponding to  $G_z\Omega_x$  and  $G_x\Omega_z$  evolved in opposite directions and stabilized to opposite values (**Fig.**  
460 **8D**, green), while all other weights decreased to 0 (**Fig. 8D**, grey). This indicates that the cell indeed  
461 learned to compute a signal proportional to  $dG_y/dt$ . Note that the weights didn't converge to values  
462 of 1 and -1 but 0.36 and -0.36: this is because the gain of the tilt signal depends not only on these  
463 weights, but also on the dynamics of tilt PC and tilt position neurons.

464 The simulated neuronal responses during tilt/translation paradigms reproduced the prominent  
465 properties of tilt- and translation-selective PC. Tilt-selective PC responded during tilt (**Fig. 8E**, middle)  
466 with a gain of 0.78 relative to tilt velocity and were primarily in phase with tilt velocity, but shifted by  
467  $11^\circ$  towards tilt position. During translation (**Fig. 8E**, left), their response gain was largely reduced (4.6  
468 times less than during tilt). Tilt position neurons also responded during tilt specifically, with a gain of

469 0.76 and a slight phase lead of 5° relative to tilt position (**Fig. 8E**, middle). Their response to translation  
470 (**Fig. 8E**, left) was also much lower (by a factor of 4.8 compared to tilt). In contrast, translation-selective  
471 cells responded during translation (**Fig. 8E**, left) with a gain of 0.97 and phase lead of 9°, and their  
472 response during tilt was reduced by a factor of 3.8 (**Fig. 8E**, middle). The simulated IO response was  
473 the inverse of that of translation-selective PC, and therefore it encoded translation. As expected, all  
474 cells responded during tilt-translation, and maintained their phase relative to tilt velocity and position  
475 (tilt PC and tilt position neurons) or translation (translation PC and IO).

476 Thus, a simple CS-driven learning rule, based on the principle of decorrelation learning, where only  
477 translation-selective cells project to the IO, is sufficient to train a neuronal network to integrate  
478 rotation signals in 3D so as to predict and cancel tilt-driven activation of the otoliths.

479

480

### Discussion

481 Olivo-cerebellar loops form a unit of cerebellar computation (Apps et al., 2018; Apps & Garwicz, 2005;  
482 Chaumont et al., 2013; De Zeeuw et al., 2011; Ekerot et al., 1991; Garwicz et al., 1998; Herzfeld et al.,  
483 2015; Ozden et al., 2009; Shadmehr, 2020; Sugihara & Quy, 2007). Here we show that two functionally  
484 distinct types of PC may implement two computational steps within a single olivo-cerebellar loop.

485 In previous studies (Angelaki et al., 2004; Laurens et al., 2013b; Laurens & Angelaki, 2020; Yakusheva  
486 et al., 2007, 2008, 2010), we have identified two distinct groups of PCs defined by their SS properties:  
487 Tilt-selective cells encode allocentric velocity relative to gravity which, when integrated, can predict  
488 the gravitational force acting on the inner ear's inertial sensors - the otoliths. Translation-selective  
489 cells encode otolith prediction error. Yet, the CS properties of both cell types are identical and  
490 proportional to the SS firing of translation-selective cells, i.e. to the otolith prediction error. This  
491 finding suggests that translation-selective PCs may control the activity of IO cells that innervate them  
492 (Chaumont et al., 2013) through their downstream projections to the fastigial or vestibular nuclei.  
493 Thus, the output of translation-selective PCs may serve as a dual function - driving behavioural  
494 responses and generating a teaching signal to maintain optimal control through the IO loop.

495 The similarity in CS response properties suggests that both types of PCs belong to a single olivo-  
496 cerebellar loop. Thus, tilt- and translation-selective cells may form a computational unit that uses its  
497 own output as a teaching signal. In this respect, they may implement the decorrelation learning rule  
498 proposed by (Dean et al., 2002, 2010; Dean & Porrill, 2014) to explain how efference copies are used  
499 to filter out self-generated actions from a sensory signal. The computations performed by tilt- and  
500 translation-selective cells are, however, more intricate than the reafference suppression function

501 because they involve a 3D non-linear spatial transformation combined with temporal integration.  
502 Indeed, our model simulations confirm that such computations can be learned using a decorrelation  
503 learning rule.

504

505 *Tilt- and translation-selective cells form a computational unit*

506 Previous studies (Angelaki et al., 2004; Laurens et al., 2013b; Laurens & Angelaki, 2020) have shown  
507 that tilt- and translation-selective cells encode the two interconnected computational steps outlined  
508 in **Fig. 1C**. Yet, their functional link had remained tentative without any established neural pathway  
509 between tilt-selective and translation-selective PCs. Alternatively, it could be that these properties  
510 arise independently in these PC types, perhaps through computations that occur elsewhere, e.g., in  
511 the granular layer or the vestibular nuclei. The current finding that both cell types receive identical IO  
512 inputs supports the notion that they are functionally linked within the same olivo-cerebellar network.

513 Our findings also provide answers to the following question: if a neuronal pathway links tilt-selective  
514 and translation-selective PCs, then, considering that this pathway is likely polysynaptic, is it overall  
515 excitatory or inhibitory? For instance, a tilt-selective cell whose SS firing encodes leftward tilt (after  
516 temporal integration) may either inhibit a translation-selective cell that encodes rightward  
517 acceleration (**Fig. 1B-D**) or activate a translation-selective cell that encodes leftward acceleration. Our  
518 finding that cells that prefer e.g. leftward tilt and rightward acceleration would receive identical IO  
519 inputs (**Fig. 5**) supports the former possibility, and suggests that the postulated anatomical link is  
520 overall inhibitory.

521

522 *Internal model computations for self-motion perception and feedback signals*

523 The concept of internal model is a classical approach for apprehending how the brain processes  
524 multisensory self-motion information, proposed as early as the late 70s (Oman, 1982; Ormsby &  
525 Young, 1977). Several quantitative models were subsequently developed in the following decades  
526 (Borah et al., 1988; Bos & Bles, 2002; Glasauer & Merfeld, 1997; Karmali & Merfeld, 2012; Laurens &  
527 Angelaki, 2011, 2017; Laurens & Droulez, 2007; Merfeld, 1995; Zupan et al., 2002), whose findings  
528 have been extensively validated by behavioural (Angelaki et al., 1999; Dakin et al., 2020; Khosravi-  
529 Hashemi et al., 2019; Laurens et al., 2010, 2011; Merfeld, 1995; Merfeld et al., 1999) and  
530 neurophysiological studies (Angelaki et al., 2004; Cullen, 2012; Cullen & Brooks, 2015; Cullen & Roy,  
531 2004; Hernández et al., 2020; Laurens et al., 2013a, 2013a; Laurens & Angelaki, 2020; Shaikh et al.,  
532 2005; Stay et al., 2019; Yakusheva et al., 2007, 2008, 2013).

533 Whereas early studies have focused on passive motion (Angelaki et al., 2004; Laurens et al., 2013a,  
534 2013a; Laurens & Angelaki, 2020; Shaikh et al., 2005; Yakusheva et al., 2007, 2008, 2013), we have  
535 proposed a more general framework (Laurens & Angelaki, 2017) in which cerebellar PCs implement a  
536 forward model of the otolith organs, and in which translation-selective cells encode the resulting  
537 sensory prediction error.

538 This theoretical hypothesis has already been supported by multiple experimental findings. First,  
539 translation-selective cells respond to translation, implying they receive sensory signals from the  
540 otoliths (or equivalent inertial signals from trunk proprioceptors), since these are the only sensors  
541 activated during passive translations. Second, their firing is reduced when other sources of  
542 information can be used to predict otolith activity; e.g., efference copy signals during active  
543 translations; Indeed, the firing of vestibular and fastigial nuclei translation-selective cells is markedly  
544 reduced (Carriot et al., 2013; Mackrous et al., 2019) - a finding which presumably generalises to  
545 translation-selective PCs in the NU. Further, responses of translation-selective cells is also diminished  
546 during tilt, during which rotation signals can be used to track head tilt relative to gravity and predict  
547 the gravitational activation of the otoliths (Glasauer & Merfeld, 1997; Laurens & Angelaki, 2017;  
548 Merfeld, 1995). Finally, this framework implies that an otolith prediction error, and a corresponding  
549 activation of translation-selective cells, should occur whenever rotation signals do not match head  
550 motion relative to vertical. We have verified this hypothesis in (Laurens et al., 2013a, 2013b), and  
551 shown that the firing of translation-selective neurons could be accurately simulated by previous  
552 quantitative models (Laurens & Angelaki, 2011).

553 Based on the internal model framework, otolith prediction errors are expected to drive a number of  
554 feedback signals that have indeed been associated with the NU. The first consequence of otolith  
555 prediction errors are behavioural responses associated with translation, such as translation  
556 perception and stabilizing eye movements. These occur, obviously, during translational motion  
557 (Angelaki et al., 1999), but also during artificial stimulation of the semicircular canals (Khosravi-  
558 Hashemi et al., 2019; Merfeld et al., 1999).

559 Next, otolith prediction errors drive a somatogravic feedback loop, which biases the tilt estimate (**Fig.**  
560 **1C**) so as to diminish otolith prediction errors at low frequencies. This feedback signal, which has been  
561 well characterized experimentally and theoretically see e.g. (Bos & Bles, 2002; Clark & Graybiel, 1966;  
562 Graybiel, 1952; Laurens et al., 2013a; Laurens & Angelaki, 2011), has been identified in the SS firing of  
563 tilt-selective cells (Laurens et al., 2013b).

564 Otolith prediction errors also drive a velocity feedback (**Fig. 1C**) that corrects rotation signals that  
565 conflict with otolith inputs: this feedback can for instance shorten the duration of rotation signals that

566 indicate incorrectly that the head tilts (Angelaki & Hess, 1995b; Hain et al., 1988; Wearne et al., 1998)  
567 or reciprocally create a rotation signal to complement the semicircular canals when the head rotates  
568 about an earth-horizontal axis (Angelaki & Hess, 1995a). Several studies have demonstrated that this  
569 feedback is abolished following lesions of the NU (Angelaki & Hess, 1995a, 1995b; Hain et al., 1988;  
570 Lee et al., 2017; Wearne et al., 1998).

571

#### 572 Neuronal and behavioural outputs of the NU

573 Translation-selective cells have been identified in multiple brain areas: the fastigial and vestibular  
574 nuclei (Angelaki et al., 2004; Hernández et al., 2020; Laurens et al., 2013a, 2013a; Laurens & Angelaki,  
575 2020; Shaikh et al., 2005; Stay et al., 2019; Yakusheva et al., 2007, 2008, 2013) and the vestibular  
576 thalamus (Dale & Cullen, 2017).

577 In contrast, tilt-selective cells have, to date, only been formally identified in the NU. This may be  
578 because identifying cells that encode rotation velocity relative to vertical requires distinguishing them  
579 from semicircular canals-driven cells that encode rotation velocity in egocentric coordinates. Tilt-  
580 selective cells and canal-driven cells have similar responses during simple rotations about earth-  
581 vertical or earth-horizontal axes, as in e.g. **Fig. 2,5**. Therefore, formally identifying tilt-selective cells  
582 requires testing their responses during multiple 3D rotations protocols, e.g., as in **Fig. 7**, which has  
583 only been done in the NU so far (Laurens et al., 2013b). For example, some rotation-selective neurons  
584 in the vestibular and fastigial nuclei (Buettner et al., 1978; Büttner et al., 2003; Siebold et al., 1997;  
585 Waespe & Henn, 1979) have been presented as tilt-selective (Mackrous et al., 2019), but it is currently  
586 unknown whether these cells encode tilt, as opposed to egocentric rotation. Note that tilt signals have  
587 been identified in the navigation system (Angelaki et al., 2020), but these cells were not tested during  
588 tilt/translation discrimination protocols, thus it is unknown whether they convey a net tilt signal.  
589 Although tilt perception is driven by a 3D internal model in humans (Clark & Graybiel, 1966; Merfeld  
590 et al., 2001; Niehof et al., 2019a, 2019b; Vingerhoets et al., 2007), whether tilt-selective cells exist  
591 outside the NU remains unknown.

592 Beyond self-motion perception, the NU innervates regions of the fastigial nucleus that are involved in  
593 attention, vigilance and hippocampal function (Fujita et al., 2020), suggesting a possible consequence  
594 of otolith prediction errors for a variety of brain functions.

595

596

597 Anatomical substrate of the olivo-cerebellar loop with the NU

598 Olivo-cerebellar loops in the NU have been studied in rabbits (Barmack & Shojaku, 1995; Fushiki &  
599 Barmack, 1997), mice (Yakhnitsa & Barmack, 2006) and cats (Kitama et al., 2014) using exclusively  
600 rotation (but not translation) stimuli. Although it is impossible to test the current hypotheses in the  
601 absence of translation stimuli, findings from these studies are consistent with the present results.  
602 First, these studies reported SS and CS modulation during tilt, but not during rotations in an earth-  
603 horizontal plane. Note that even translation-selective cells show a substantial modulation during tilt  
604 (**Fig. 3A, Fig. 5**). It is thus possible that neurons recorded in previous studies reflected a mixture of tilt-  
605 selective and translation-selective cells. In fact, one study (Kitama et al., 2014) noted that NU cells  
606 could respond in phase with either tilt position or velocity. Considering that tilt-selective cells encode  
607 velocity (Laurens & Angelaki, 2020), 'velocity' cells likely correspond to tilt-selective cells, whereas  
608 'position' cells likely correspond to translation-selective cells. This interpretation is corroborated by  
609 the SS modulation gain during tilt at 0.5Hz: 133 and 64 spk/s/G respectively for 'velocity' and 'position'  
610 cells respectively in (Kitama et al., 2014), that match our recordings (**Fig. 3A**). Furthermore, previous  
611 studies also found that CSs occur in antiphase with SSs, in agreement with our observations (**Fig. 5**).  
612 Altogether, these similarities indicate that the NU PCs reported to be modulated by tilt in (Barmack &  
613 Shojaku, 1995; Fushiki & Barmack, 1997; Kitama et al., 2014; Yakhnitsa & Barmack, 2006) correspond  
614 to tilt- and translation-selective cells.

615 The medial portion of the NU receives projections from two regions of the IO. The first, which is  
616 composed of the dorsal cap and ventrolateral outgrowth, carries visual optokinetic signals (Barmack  
617 & Hess, 1980; Leonard et al., 1988) to a small medial portion of the nodulus. Since our experiments  
618 were performed in darkness, this region is unlikely to account for the CS responses studied here. The  
619 second IO region is the beta nucleus (Barmack, Fagerson, Fredette, et al., 1993; Voogd et al., 1996),  
620 which receives projections from the medial and descending vestibular nuclei (Balaban & Beryozkin,  
621 1994; Barmack, Fagerson, & Errico, 1993; Gerrits et al., 1985; Saint-Cyr & Courville, 1979; Turecek &  
622 Regehr, 2020) and the parasolitary nucleus (Barmack, 2006; Barmack & Yakhnitsa, 2000). In turn, the  
623 medial and descending vestibular nuclei receive projection from the NU (Bernard, 1987; Epema et al.,  
624 1985; Shojaku et al., 1987; Wylie et al., 1994), as well as the parasolitary nucleus (Barmack,  
625 unpublished observations reported in (Barmack & Yakhnitsa, 2000), and R. Sillitoe, personal  
626 communication). Thus, the anatomical substrate of the olivo-cerebellar loop involving tilt and  
627 translation-selective cells may include a projection of the NU to the beta nucleus through the medial  
628 and descending vestibular and parasolitary nuclei. In agreement with this hypothesis, translation-  
629 selective cells exist in the vestibular nuclei (Angelaki et al., 2004; Zhou et al., 2006); the firing of  
630 neurons in the parasolitary and beta nuclei is similar to the CS responses in the NU (Barmack, Fagerson,

631 Fredette, et al., 1993; Barmack & Yakhnitsa, 2000), and Fos expression studies indicate that the beta  
632 nucleus is activated by linear accelerations (Li et al., 2013).

633

634 Conclusion

635 From an experimenter's point of view, linking neural circuits and theoretical predictions may appear  
636 an arduous if not vain undertaking, since abstract concepts such as internal models and Kalman  
637 filtering may seem too far remote from physiological reality, if not plainly "too nice". Indeed, we too  
638 are amazed that the vestibulo-cerebellar circuit should consistently reflect this theorized  
639 computations. And yet, these findings should not come as a complete surprise, since behavioural  
640 studies have consistently shown that the brain implements the building blocks of internal models,  
641 which are nicely mathematically tractable in a well-defined problem such as tilt/translation  
642 discrimination. We can only conclude that when theoretical concepts have passed the test of decades  
643 of scrutiny, then we should expect to find their embodiment in neuronal circuits. We hope that the  
644 example of the vestibular field may inspire physiologists and system scientists in other fields where  
645 similar theoretical frameworks exist.

646

647 **Acknowledgements**

648 The work was supported by NIH grant DC004260.



649 **Methods**650 Animals

651 Three male rhesus Macaques, aged 3, 4 and 9 years, were used in the study. The animals were pair-  
652 housed in a vivarium under normal day/night cycle illumination. Experimental procedures were in  
653 accordance with US National Institutes of Health guidelines and approved by the Animal Studies  
654 Committee at Washington University in St Louis (approval n°20100230).

655 Experimental procedures and neuronal recordings

656 Experimental procedures were described in detail in (Laurens et al., 2013a, 2013b). In summary,  
657 animals were installed in primate chairs that were installed on a 3-axes rotator mounted on a linear  
658 (Acutronics Inc, Pittsburg, PA) sled. We recorded neurons extracellularly using epoxy-coated tungsten  
659 electrodes (5 or 20 M $\Omega$  impedance; FHC, Bowdoinham, ME). Recording locations were determined  
660 stereotaxically and relative to the abducens nucleus. Raw spiking data was sorted offline using  
661 custom Matlab scripts, based on spike amplitude and principal components analysis. In this study, we  
662 included only neurons where CS firing could be isolated consistently across trials, and where CS were  
663 followed by a pause in SS firing for at least 10 ms.

664 Experimental protocols

665 Sinusoidal tilt and translation stimuli (**Fig. 2A**) consisted in translation (peak acceleration = 0.2 g, with  
666  $g = 9.81 \text{ m/s}^2$ ) or tilt (peak tilt = 11.5°) oscillations at 0.5 Hz, or combinations of these stimuli (out of  
667 phase: tilt-translation or in phase: tilt+translation). Stimuli could be delivered along the head's naso-  
668 occipital axis (forward/backward translation and pitch tilt), lateral axis (left/right translation and roll  
669 tilt) or along intermediate axes. We recorded the response of each cell using stimuli along at least two  
670 head axes.

671 Tilt while rotating (TWR) (Laurens et al., 2013a) consists in rotating the setup about a fixed earth-  
672 vertical axis at a constant velocity of 45°/s. During this rotation, animals were tilted back and forth  
673  $\pm 10^\circ$  along one plane (i.e. pitch, roll or intermediate) about the vertical axis. Tilt movements were brief  
674 movements (peak velocity 20°/s, acceleration 50°/s<sup>2</sup>, duration 1.4s) that were separated by 30s of  
675 fixed tilt.

676 Off-vertical axis rotation (OVAR) (Laurens et al., 2013b) consisted in tilting the animal by 10°, and then  
677 rotating them around the head's vertical axis at 180°/s (peak acceleration: 90°/s<sup>2</sup>) for 80s. This resulted  
678 in the head tilting in a sequence (nose up, left ear down, nose down, right ear down, nose up) which  
679 is equivalent to out-of-phase oscillations in pitch and roll, with 10° peak tilt, at 0.5 Hz.

680 Data analysis

681 SS and CS firing were analysed using the same methods as in (Laurens et al., 2013a, 2013b). We also  
 682 refer the reader to (Laurens & Angelaki, 2016) for an in-depth presentation of the analysis of sinusoidal  
 683 tilt and translation stimuli. In this section, we present some analyses that were specifically developed  
 684 or modified in the present study.

685 *Modulation amplitude:* The only difference between the analysis of SS and CS was the way modulation  
 686 amplitude was computed. To quantify the modulation of SS, we fitted firing histograms with a rectified  
 687 sinusoid function:  $FR(t) = \max(0; FR_0 + A \cdot \cos(\pi \cdot \omega \cdot t + \phi))$  where  $\omega$  is the stimulus frequency in Hz,  $A$  and  
 688  $\phi$  the response amplitude and phase and  $FR_0$  the cell's baseline firing. To quantify the modulation of  
 689 CS, we performed a simple Fourier transform, which is equivalent to fitting firing histograms with a  
 690 sinusoid  $FR(t) = FR_0 + A \cdot \cos(\pi \cdot \omega \cdot t + \phi)$ , without rectification. We chose this approach because using a  
 691 rectified function yields more accurate results for cells where the firing becomes 'less than 0' in the  
 692 trough of the firing histograms, but is unreliable when cells discharge a low number of spikes, which  
 693 is the case with CS. Note that the choice of method will not alter our findings that CS fire preferentially  
 694 during translation, since with use the same method to analyse CS response during tilt and translation,  
 695 and also since **Fig. 5**, which is based on raw spiking histograms, supports our conclusion.

696 *Response PD and phase:* In **Fig. 4**, we summarize the cells' firing properties by computing the PD and  
 697 response phase of SS and CS. For instance, a cell may respond to leftward acceleration with a phase  
 698 lead of  $10^\circ$ . However, it is equivalent to state that this cell responds to rightward acceleration with a  
 699 phase lead of  $-170^\circ$ . In order to express the response PD and phase of SS and CS in a coherent manner,  
 700 we adopt the following procedure.

701 First, we compute the PD and phase of SS such that the response phase during tilt is always within  
 702  $54 \pm 90^\circ$  for tilt-selective cells, such that the response phase during translation is always within  $\pm 90^\circ$   
 703 for other cells, i.e. we reverse both the PD and phase when the phase falls out of this interval. We  
 704 chose this convention because tilt-selective cells respond preferentially to tilt, with an average lead of  
 705  $54^\circ$  relative to position, whereas other cells respond preferentially or equally to translation, with an  
 706 phase of  $\sim 0$  (see (Laurens et al., 2013b)). Note that this convention has no impact on our statistical  
 707 analyses but only serves to make results clearer (e.g. in **Fig. 4C**).

708 Next, we compute the PD and phase of CS, independently from the SS response. In a second step, if  
 709 the PD of SS and CS are more than  $90^\circ$  apart, we revert both the PD and phase of CS.

710 In absolute terms, these conventions do not change how we measure the SS and CS responses, since  
 711 reversing both the PD and phase results in an equivalent description of the response. However, from

712 a statistical point of view, they imply that (1) the absolute difference between the PD of SS and CS is  
 713 always less than 90° (**Fig. 4A,B**), the phase of SS is expressed as a circular variable with a periodicity of  
 714 180° whereas the phase of CS is a circular variable with a periodicity of 360° (**Fig. 4C,D**). As a result,  
 715 cell-to-cell variations in response phase of SS have a higher impact, such that we could not compute  
 716 the confidence interval of SS in **Fig. 4D**. However, these confidence intervals were computed using the  
 717 same method and a larger number of cells in (Laurens et al., 2013b).

718 *Regression analysis:* We tested which cell populations control CS firing by performing a multiple  
 719 regression analysis. We concatenated the CS firing histogram during translation, tilt and tilt-translation  
 720 (averaged across all translation-, tilt-, and GIA-selective cells, and with 20 times bin each) into a single  
 721 vector  $CS_i$  with 60 bins. We also computed similar SS firing histograms for translation-, tilt- and GIA-  
 722 selective cells:  $SS_i^{trans}$ ,  $SS_i^{trans}$  and  $SS_i^{GIA}$ . We used a quadratic regression model:

$$723 \quad CS_i = a + b^{trans} \cdot SS_i^{trans} + c^{trans} \cdot (SS_i^{trans})^2 + b^{tilt} \cdot SS_i^{tilt} + c^{tilt} \cdot (SS_i^{tilt})^2 + b^{GIA} \cdot SS_i^{GIA} + c^{GIA} \cdot (SS_i^{GIA})^2$$

724 We evaluated the goodness of fit of the regression by computing the squared coefficient of correlation  
 725  $R^2 = 1 - SSR/SS_{tot}$  where SSR is the sum of squared residuals and  $SS_{tot}$  the variance of  $CS_i$ . To measure  
 726 the contribution of each SS response type, we computed partials  $R^2$ , e.g. for translation-selective cells,  
 727 we computed  $pR_{trans}^2 = 1 - SSR/SSR_{trans}$ , where  $SSR_{trans}$  is the sum of squared residuals obtained when  
 728 translation-selective cells are excluded from the regression. A large/small  $pR^2$  indicates that including  
 729 a given response type has a large/small impact on the regression's goodness of fit, implying that SS  
 730 from the corresponding population of PC contribute to a large/small extent to controlling CS firing.  
 731 We used a shuffling approach to estimate the confidence intervals of  $pR^2$ : we computed 10000  
 732 shuffled values of  $pR_{trans}^2$ , for each of which the vector  $SS_i^{trans}$  was shuffled, and defined the confidence  
 733 interval (at  $\alpha = 1\%$ ) as the 99-percentile of the distribution of shuffled values. We performed the same  
 734 computation for  $pR_{tilt}^2$  and  $pR_{GIA}^2$ . We found that the 99-percentile is equal to 0.16 in all cases.

735

736 **References**

- 737 Albus, J. S. (1971). A theory of cerebellar function. *Mathematical Biosciences*, 10(1–2), 25–61.  
738 [https://doi.org/10.1016/0025-5564\(71\)90051-4](https://doi.org/10.1016/0025-5564(71)90051-4)
- 739 Angelaki, D. E., & Hess, B. J. (1995a). Lesion of the nodulus and ventral uvula abolish steady-state off-  
740 vertical axis otolith response. *Journal of Neurophysiology*, 73(4), 1716–1720.  
741 <https://doi.org/10.1152/jn.1995.73.4.1716>
- 742 Angelaki, D. E., & Hess, B. J. (1995b). Inertial representation of angular motion in the vestibular system  
743 of rhesus monkeys. II. Otolith-controlled transformation that depends on an intact cerebellar  
744 nodulus. *Journal of Neurophysiology*, 73(5), 1729–1751.  
745 <https://doi.org/10.1152/jn.1995.73.5.1729>
- 746 Angelaki, D. E., McHenry, M. Q., Dickman, J. D., Newlands, S. D., & Hess, B. J. M. (1999). Computation  
747 of Inertial Motion: Neural Strategies to Resolve Ambiguous Otolith Information. *The Journal*  
748 *of Neuroscience*, 19(1), 316–327. <https://doi.org/10.1523/JNEUROSCI.19-01-00316.1999>
- 749 Angelaki, D. E., Ng, J., Abrego, A. M., Cham, H. X., Asproдини, E. K., Dickman, J. D., & Laurens, J. (2020).  
750 A gravity-based three-dimensional compass in the mouse brain. *Nature Communications*,  
751 11(1), 1855. <https://doi.org/10.1038/s41467-020-15566-5>
- 752 Angelaki, D. E., Shaikh, A. G., Green, A. M., & Dickman, J. D. (2004). Neurons compute internal models  
753 of the physical laws of motion. *Nature*, 430(6999), 560–564.  
754 <https://doi.org/10.1038/nature02754>
- 755 Apps, R., & Garwicz, M. (2005). Anatomical and physiological foundations of cerebellar information  
756 processing. *Nature Reviews Neuroscience*, 6(4), 297–311. <https://doi.org/10.1038/nrn1646>
- 757 Apps, R., Hawkes, R., Aoki, S., Bengtsson, F., Brown, A. M., Chen, G., Ebner, T. J., Isope, P., Jörntell, H.,  
758 Lackey, E. P., Lawrenson, C., Lumb, B., Schonewille, M., Sillitoe, R. V., Spaeth, L., Sugihara, I.,  
759 Valera, A., Voogd, J., Wylie, D. R., & Ruigrok, T. J. H. (2018). Cerebellar Modules and Their Role  
760 as Operational Cerebellar Processing Units. *The Cerebellum*, 17(5), 654–682.  
761 <https://doi.org/10.1007/s12311-018-0952-3>
- 762 Balaban, C. D., & Beryozkin, G. (1994). Organization of vestibular nucleus projections to the caudal  
763 dorsal cap of kooy in rabbits. *Neuroscience*, 62(4), 1217–1236. [https://doi.org/10.1016/0306-4522\(94\)90354-9](https://doi.org/10.1016/0306-4522(94)90354-9)
- 765 Barmack, N. H. (2006). Inferior olive and oculomotor system. In *Progress in Brain Research* (Vol. 151,  
766 pp. 269–291). Elsevier. [https://doi.org/10.1016/S0079-6123\(05\)51009-4](https://doi.org/10.1016/S0079-6123(05)51009-4)
- 767 Barmack, N. H., Fagerson, M., & Errico, P. (1993). Cholinergic projection to the dorsal cap of the inferior  
768 olive of the rat, rabbit, and monkey. *The Journal of Comparative Neurology*, 328(2), 263–281.  
769 <https://doi.org/10.1002/cne.903280208>
- 770 Barmack, N. H., Fagerson, M., Fredette, B. J., Mugnaini, E., & Shojaku, H. (1993). Activity of neurons in  
771 the beta nucleus of the inferior olive of the rabbit evoked by natural vestibular stimulation.  
772 *Experimental Brain Research*, 94(2). <https://doi.org/10.1007/BF00230288>
- 773 Barmack, N. H., & Hess, D. T. (1980). Multiple-unit activity evoked in dorsal cap of inferior olive of the  
774 rabbit by visual stimulation. *Journal of Neurophysiology*, 43(1), 151–164.  
775 <https://doi.org/10.1152/jn.1980.43.1.151>
- 776 Barmack, N. H., & Shojaku, H. (1995). Vestibular and visual climbing fiber signals evoked in the uvula-  
777 nodulus of the rabbit cerebellum by natural stimulation. *Journal of Neurophysiology*, 74(6),  
778 2573–2589. <https://doi.org/10.1152/jn.1995.74.6.2573>
- 779 Barmack, N. H., & Yakhnitsa, V. (2000). Vestibular Signals in the Parasolitary Nucleus. *Journal of*  
780 *Neurophysiology*, 83(6), 3559–3569. <https://doi.org/10.1152/jn.2000.83.6.3559>
- 781 Bernard, J.-F. (1987). Topographical organization of olivocerebellar and corticonuclear connections in  
782 the rat? An WGA-HRP study: I. Lobules IX, X, and the flocculus. *The Journal of Comparative*  
783 *Neurology*, 263(2), 241–258. <https://doi.org/10.1002/cne.902630207>
- 784 Borah, J., Young, L. R., & Curry, R. E. (1988). Optimal Estimator Model for Human Spatial Orientation  
785 <sup>a</sup>. *Annals of the New York Academy of Sciences*, 545(1), 51–73. <https://doi.org/10.1111/j.1749-6632.1988.tb19555.x>

- 787 Bos, J. E., & Bles, W. (2002). Theoretical considerations on canal-otolith interaction and an observer  
788 model. *Biological Cybernetics*, *86*(3), 191–207. <https://doi.org/10.1007/s00422-001-0289-7>
- 789 Buettner, U. W., Buttner, U., & Henn, V. (1978). Transfer characteristics of neurons in vestibular nuclei  
790 of the alert monkey. *Journal of Neurophysiology*, *41*(6), 1614–1628.  
791 <https://doi.org/10.1152/jn.1978.41.6.1614>
- 792 Büttner, U., Glasauer, S., Glonti, L., Guan, Y., Kipiani, E., Kleine, J., Siebold, C., Tchelidze, T., & Wilden,  
793 A. (2003). Multimodal Signal Integration in Vestibular Neurons of the Primate Fastigial  
794 Nucleus. *Annals of the New York Academy of Sciences*, *1004*(1), 241–251.  
795 <https://doi.org/10.1196/annals.1303.021>
- 796 Carriot, J., Brooks, J. X., & Cullen, K. E. (2013). Multimodal Integration of Self-Motion Cues in the  
797 Vestibular System: Active versus Passive Translations. *Journal of Neuroscience*, *33*(50), 19555–  
798 19566. <https://doi.org/10.1523/JNEUROSCI.3051-13.2013>
- 799 Cerminara, N. L., Garwicz, M., Darch, H., Houghton, C., Marple-Horvat, D. E., & Apps, R. (2020). *Action-*  
800 *based organization and function of cerebellar cortical microcircuits* [Preprint]. Neuroscience.  
801 <https://doi.org/10.1101/2020.04.04.025387>
- 802 Chaumont, J., Guyon, N., Valera, A. M., Dugue, G. P., Popa, D., Marcaggi, P., Gautheron, V., Reibel-  
803 Foisset, S., Dieudonne, S., Stephan, A., Barrot, M., Cassel, J.-C., Dupont, J.-L., Doussau, F.,  
804 Poulain, B., Selimi, F., Lena, C., & Isope, P. (2013). Clusters of cerebellar Purkinje cells control  
805 their afferent climbing fiber discharge. *Proceedings of the National Academy of Sciences*,  
806 *110*(40), 16223–16228. <https://doi.org/10.1073/pnas.1302310110>
- 807 Clark, B., & Graybiel, A. (1966). Factors Contributing to the Delay in the Perception of the Oculogravic  
808 Illusion. *The American Journal of Psychology*, *79*(3), 377. <https://doi.org/10.2307/1420878>
- 809 Cullen, K. E. (2012). The vestibular system: Multimodal integration and encoding of self-motion for  
810 motor control. *Trends in Neurosciences*, *35*(3), 185–196.  
811 <https://doi.org/10.1016/j.tins.2011.12.001>
- 812 Cullen, K. E., & Brooks, J. X. (2015). Neural Correlates of Sensory Prediction Errors in Monkeys:  
813 Evidence for Internal Models of Voluntary Self-Motion in the Cerebellum. *The Cerebellum*,  
814 *14*(1), 31–34. <https://doi.org/10.1007/s12311-014-0608-x>
- 815 Cullen, K. E., & Roy, J. E. (2004). Signal Processing in the Vestibular System During Active Versus Passive  
816 Head Movements. *Journal of Neurophysiology*, *91*(5), 1919–1933.  
817 <https://doi.org/10.1152/jn.00988.2003>
- 818 Dakin, C. J., Kumar, P., Forbes, P. A., Peters, A., & Day, B. L. (2020). Variance based weighting of  
819 multisensory head rotation signals for verticality perception. *PLOS ONE*, *15*(1), e0227040.  
820 <https://doi.org/10.1371/journal.pone.0227040>
- 821 Dale, A., & Cullen, K. E. (2017). The Ventral Posterior Lateral Thalamus Preferentially Encodes  
822 Externally Applied Versus Active Movement: Implications for Self-Motion Perception. *Cerebral*  
823 *Cortex*, *29*(1), 305–318. <https://doi.org/10.1093/cercor/bhx325>
- 824 De Zeeuw, C. I., Hoebeek, F. E., Bosman, L. W. J., Schonewille, M., Witter, L., & Koekkoek, S. K. (2011).  
825 Spatiotemporal firing patterns in the cerebellum. *Nature Reviews Neuroscience*, *12*(6), 327–  
826 344. <https://doi.org/10.1038/nrn3011>
- 827 Dean, P., & Porrill, J. (2014). Decorrelation Learning in the Cerebellum. In *Progress in Brain Research*  
828 (Vol. 210, pp. 157–192). Elsevier. <https://doi.org/10.1016/B978-0-444-63356-9.00007-8>
- 829 Dean, P., Porrill, J., Ekerot, C.-F., & Jörntell, H. (2010). The cerebellar microcircuit as an adaptive filter:  
830 Experimental and computational evidence. *Nature Reviews Neuroscience*, *11*(1), 30–43.  
831 <https://doi.org/10.1038/nrn2756>
- 832 Dean, P., Porrill, J., & Stone, J. V. (2002). Decorrelation control by the cerebellum achieves oculomotor  
833 plant compensation in simulated vestibulo-ocular reflex. *Proceedings of the Royal Society of*  
834 *London. Series B: Biological Sciences*, *269*(1503), 1895–1904.  
835 <https://doi.org/10.1098/rspb.2002.2103>
- 836 Einstein, A. (1907). Über das Relativitätsprinzip und die aus demselben gezogenen Folgerungen, *Jahrb.*  
837 *D. Radioaktivität u. Elektronik. IV*, 454.

- 838 Ekerot, C. F., Garwicz, M., & Schouenborg, J. (1991). Topography and nociceptive receptive fields of  
839 climbing fibres projecting to the cerebellar anterior lobe in the cat. *The Journal of Physiology*,  
840 441(1), 257–274. <https://doi.org/10.1113/jphysiol.1991.sp018750>
- 841 Epema, A. H., Guldemond, J. M., & Voogd, J. (1985). Reciprocal connections between the caudal vermis  
842 and the vestibular nuclei in the rabbit. *Neuroscience Letters*, 57(3), 273–278.  
843 [https://doi.org/10.1016/0304-3940\(85\)90504-X](https://doi.org/10.1016/0304-3940(85)90504-X)
- 844 Fujita, H., Kodama, T., & du Lac, S. (2020). Modular output circuits of the fastigial nucleus for diverse  
845 motor and nonmotor functions of the cerebellar vermis. *ELife*, 9, e58613.  
846 <https://doi.org/10.7554/eLife.58613>
- 847 Fushiki, H., & Barmack, N. H. (1997). Topography and Reciprocal Activity of Cerebellar Purkinje Cells in  
848 the Uvula-Nodulus Modulated by Vestibular Stimulation. *Journal of Neurophysiology*, 78(6),  
849 3083–3094. <https://doi.org/10.1152/jn.1997.78.6.3083>
- 850 Garwicz, M., Ekerot, C.-F., & Jörntell, H. (1998). Organizational Principles of Cerebellar Neuronal  
851 Circuitry. *Physiology*, 13(1), 26–32. <https://doi.org/10.1152/physiologyonline.1998.13.1.26>
- 852 Gerrits, N. M., Voogd, J., & Magras, I. N. (1985). Vestibular afferents of the inferior olive and the  
853 vestibulo-olivo-cerebellar climbing fiber pathway to the flocculus in the cat. *Brain Research*,  
854 332(2), 325–336. [https://doi.org/10.1016/0006-8993\(85\)90601-8](https://doi.org/10.1016/0006-8993(85)90601-8)
- 855 Glasauer, S., & Merfeld, D. M. (1997). Modelling three-dimensional vestibular responses during  
856 complex motion stimulation. In *Three-dimensional kinematics of eye, head and limb*  
857 *movements* (pp. 387–398).
- 858 Graybiel, A. (1952). Oculogravic illusion. *AMA Archives of Ophthalmology*, 48(5), 605–615.
- 859 Green, A. M., Shaikh, A. G., & Angelaki, D. E. (2005). Sensory vestibular contributions to constructing  
860 internal models of self-motion. *Journal of Neural Engineering*, 2(3), S164–S179.  
861 <https://doi.org/10.1088/1741-2560/2/3/S02>
- 862 Hain, T. C., Zee, D. S., & Maria, B. L. (1988). Tilt Suppression of Vestibulo-ocular Reflex in Patients with  
863 Cerebellar Lesions. *Acta Oto-Laryngologica*, 105(1–2), 13–20.  
864 <https://doi.org/10.3109/00016488809119440>
- 865 Hernández, R. G., De Zeeuw, C. I., Zhang, R., Yakusheva, T. A., & Blazquez, P. M. (2020). Translation  
866 information processing is regulated by protein kinase C-dependent mechanism in Purkinje  
867 cells in murine posterior vermis. *Proceedings of the National Academy of Sciences*, 202002177.  
868 <https://doi.org/10.1073/pnas.2002177117>
- 869 Herzfeld, D. J., Kojima, Y., Soetedjo, R., & Shadmehr, R. (2015). Encoding of action by the Purkinje cells  
870 of the cerebellum. *Nature*, 526(7573), 439–442. <https://doi.org/10.1038/nature15693>
- 871 Herzfeld, D. J., Kojima, Y., Soetedjo, R., & Shadmehr, R. (2018). Encoding of error and learning to  
872 correct that error by the Purkinje cells of the cerebellum. *Nature Neuroscience*, 21(5), 736–  
873 743. <https://doi.org/10.1038/s41593-018-0136-y>
- 874 Hess, B. J. M., & Angelaki, D. E. (1999). Oculomotor Control of Primary Eye Position Discriminates  
875 Between Translation and Tilt. *Journal of Neurophysiology*, 81(1), 394–398.  
876 <https://doi.org/10.1152/jn.1999.81.1.394>
- 877 Ito, M. (2006). Cerebellar circuitry as a neuronal machine. *Progress in Neurobiology*, 78(3–5), 272–  
878 303. <https://doi.org/10.1016/j.pneurobio.2006.02.006>
- 879 Karmali, F., & Merfeld, D. M. (2012). A distributed, dynamic, parallel computational model: The role  
880 of noise in velocity storage. *Journal of Neurophysiology*, 108(2), 390–405.  
881 <https://doi.org/10.1152/jn.00883.2011>
- 882 Kawato, M. (1999). Internal models for motor control and trajectory planning. *Current Opinion in*  
883 *Neurobiology*, 9(6), 718–727. [https://doi.org/10.1016/S0959-4388\(99\)00028-8](https://doi.org/10.1016/S0959-4388(99)00028-8)
- 884 Khosravi-Hashemi, N., Forbes, P. A., Dakin, C. J., & Blouin, J. (2019). Virtual signals of head rotation  
885 induce gravity-dependent inferences of linear acceleration. *The Journal of Physiology*,  
886 597(21), 5231–5246. <https://doi.org/10.1113/JP278642>
- 887 Kimpo, R. R., Rinaldi, J. M., Kim, C. K., Payne, H. L., & Raymond, J. L. (2014). Gating of neural error  
888 signals during motor learning. *ELife*, 3, e02076. <https://doi.org/10.7554/eLife.02076>

- 889 Kitama, T., Komagata, J., Ozawa, K., Suzuki, Y., & Sato, Y. (2014). Plane-specific Purkinje cell responses  
890 to vertical head rotations in the cat cerebellar nodulus and uvula. *Journal of Neurophysiology*,  
891 *112*(3), 644–659. <https://doi.org/10.1152/jn.00029.2014>
- 892 Kostadinov, D., Beau, M., Pozo, M. B., & Häusser, M. (2019). Predictive and reactive reward signals  
893 conveyed by climbing fiber inputs to cerebellar Purkinje cells. *Nature Neuroscience*, *22*(6),  
894 950–962. <https://doi.org/10.1038/s41593-019-0381-8>
- 895 Laurens, J., & Angelaki, D. E. (2011). The functional significance of velocity storage and its dependence  
896 on gravity. *Experimental Brain Research*, *210*(3–4), 407–422. [https://doi.org/10.1007/s00221-](https://doi.org/10.1007/s00221-011-2568-4)  
897 [011-2568-4](https://doi.org/10.1007/s00221-011-2568-4)
- 898 Laurens, J., & Angelaki, D. E. (2016). How the Vestibulocerebellum Builds an Internal Model of Self-  
899 motion. In *The Neuronal Codes of the Cerebellum* (pp. 97–115). Elsevier.  
900 <https://doi.org/10.1016/B978-0-12-801386-1.00004-6>
- 901 Laurens, J., & Angelaki, D. E. (2017). A unified internal model theory to resolve the paradox of active  
902 versus passive self-motion sensation. *Elife*, *6*, e28074.
- 903 Laurens, J., & Angelaki, D. E. (2020). Simple spike dynamics of Purkinje cells in the macaque vestibulo-  
904 cerebellum during passive whole-body self-motion. *Proceedings of the National Academy of*  
905 *Sciences*, *117*(6), 3232–3238. <https://doi.org/10.1073/pnas.1915873117>
- 906 Laurens, J., & Droulez, J. (2007). Bayesian processing of vestibular information. *Biological Cybernetics*,  
907 *96*(4), 389–404.
- 908 Laurens, J., Meng, H., & Angelaki, D. E. (2013a). Computation of linear acceleration through an internal  
909 model in the macaque cerebellum. *Nature Neuroscience*, *16*(11), 1701–1708.  
910 <https://doi.org/10.1038/nn.3530>
- 911 Laurens, J., Meng, H., & Angelaki, D. E. (2013b). Neural Representation of Orientation Relative to  
912 Gravity in the Macaque Cerebellum. *Neuron*, *80*(6), 1508–1518.  
913 <https://doi.org/10.1016/j.neuron.2013.09.029>
- 914 Laurens, J., Strauman, D., & Hess, B. J. (2011). Spinning versus Wobbling: How the Brain Solves a  
915 Geometry Problem. *Journal of Neuroscience*, *31*(22), 8093–8101.  
916 <https://doi.org/10.1523/JNEUROSCI.5900-10.2011>
- 917 Laurens, J., Straumann, D., & Hess, B. J. M. (2010). Processing of Angular Motion and Gravity  
918 Information Through an Internal Model. *Journal of Neurophysiology*, *104*(3), 1370–1381.  
919 <https://doi.org/10.1152/jn.00143.2010>
- 920 Lee, S.-U., Choi, J.-Y., Kim, H.-J., Park, J.-J., Zee, D. S., & Kim, J.-S. (2017). Impaired Tilt Suppression of  
921 Post-Rotatory Nystagmus and Cross-Coupled Head-Shaking Nystagmus in Cerebellar Lesions:  
922 Image Mapping Study. *The Cerebellum*, *16*(1), 95–102. [https://doi.org/10.1007/s12311-016-](https://doi.org/10.1007/s12311-016-0772-2)  
923 [0772-2](https://doi.org/10.1007/s12311-016-0772-2)
- 924 Leonard, C. S., Simpson, J. I., & Graf, W. (1988). Spatial organization of visual messages of the rabbit's  
925 cerebellar flocculus. I. Typology of inferior olive neurons of the dorsal cap of Kooy. *Journal of*  
926 *Neurophysiology*, *60*(6), 2073–2090. <https://doi.org/10.1152/jn.1988.60.6.2073>
- 927 Li, C., Han, L., Ma, C.-W., Lai, S.-K., Lai, C.-H., Shum, D. K. Y., & Chan, Y.-S. (2013). Maturation profile of  
928 inferior olivary neurons expressing ionotropic glutamate receptors in rats: Role in coding  
929 linear accelerations. *Brain Structure and Function*, *218*(4), 833–850.  
930 <https://doi.org/10.1007/s00429-012-0432-3>
- 931 Lisberger, S. (1988). The neural basis for learning of simple motor skills. *Science*, *242*(4879), 728–735.  
932 <https://doi.org/10.1126/science.3055293>
- 933 Mackrous, I., Carriot, J., Jamali, M., & Cullen, K. E. (2019). Cerebellar Prediction of the Dynamic Sensory  
934 Consequences of Gravity. *Current Biology*, *29*(16), 2698–2710.e4.  
935 <https://doi.org/10.1016/j.cub.2019.07.006>
- 936 Marr, D. (1969). A theory of cerebellar cortex. *The Journal of Physiology*, *202*(2), 437–470.  
937 <https://doi.org/10.1113/jphysiol.1969.sp008820>

- 938 Merfeld, D. M. (1995). Modeling the vestibulo-ocular reflex of the squirrel monkey during eccentric  
939 rotation and roll tilt. *Experimental Brain Research*, 106(1).  
940 <https://doi.org/10.1007/BF00241362>
- 941 Merfeld, D. M., Zupan, L. H., & Gifford, C. A. (2001). Neural Processing of Gravito-Inertial Cues in  
942 Humans. II. Influence of the Semicircular Canals During Eccentric Rotation. *Journal of*  
943 *Neurophysiology*, 85(4), 1648–1660. <https://doi.org/10.1152/jn.2001.85.4.1648>
- 944 Merfeld, D. M., Zupan, L., & Peterka, R. J. (1999). Humans use internal models to estimate gravity and  
945 linear acceleration. *Nature*, 398(6728), 615–618. <https://doi.org/10.1038/19303>
- 946 Nguyen-Vu, T. B., Kimpo, R. R., Rinaldi, J. M., Kohli, A., Zeng, H., Deisseroth, K., & Raymond, J. L. (2013).  
947 Cerebellar Purkinje cell activity drives motor learning. *Nature Neuroscience*, 16(12), 1734.
- 948 Niehof, N., Perdreau, F., Koppen, M., & Medendorp, W. P. (2019a). Contributions of optostatic and  
949 optokinetic cues to the perception of vertical. *Journal of Neurophysiology*, 122(2), 480–489.  
950 <https://doi.org/10.1152/jn.00740.2018>
- 951 Niehof, N., Perdreau, F., Koppen, M., & Medendorp, W. P. (2019b). Time course of the subjective visual  
952 vertical during sustained optokinetic and galvanic vestibular stimulation. *Journal of*  
953 *Neurophysiology*, 122(2), 788–796. <https://doi.org/10.1152/jn.00083.2019>
- 954 Oman, C. M. (1982). A heuristic mathematical model for the dynamics of sensory conflict and motion  
955 sickness. *Acta Oto-Laryngologica*, 94(sup392), 4–44.
- 956 Ormsby, C. C., & Young, L. R. (1977). Integration of semicircular canal and otolith information for  
957 multisensory orientation stimuli. *Mathematical Biosciences*, 34(1–2), 1–21.
- 958 Ozden, I., Sullivan, M. R., Lee, H. M., & Wang, S. S.-H. (2009). Reliable Coding Emerges from  
959 Coactivation of Climbing Fibers in Microbands of Cerebellar Purkinje Neurons. *Journal of*  
960 *Neuroscience*, 29(34), 10463–10473. <https://doi.org/10.1523/JNEUROSCI.0967-09.2009>
- 961 Saint-Cyr, J. A., & Courville, J. (1979). Projection from the vestibular nuclei to the inferior olive in the  
962 cat: An autoradiographic and horseradish peroxidase study. *Brain Research*, 165(2), 189–200.  
963 [https://doi.org/10.1016/0006-8993\(79\)90553-5](https://doi.org/10.1016/0006-8993(79)90553-5)
- 964 Shadmehr, R. (2020). *Population coding in the cerebellum and its implications for learning from error*  
965 [Preprint]. Neuroscience. <https://doi.org/10.1101/2020.05.18.102376>
- 966 Shaikh, A. G., Green, A. M., Ghasia, F. F., Newlands, S. D., Dickman, J. D., & Angelaki, D. E. (2005).  
967 Sensory Convergence Solves a Motion Ambiguity Problem. *Current Biology*, 15(18), 1657–  
968 1662. <https://doi.org/10.1016/j.cub.2005.08.009>
- 969 Shojaku, H., Sato, Y., Ikarashi, K., & Kawasaki, T. (1987). Topographical distribution of Purkinje cells in  
970 the uvula and the nodulus projecting to the vestibular nuclei in cats. *Brain Research*, 416(1),  
971 100–112. [https://doi.org/10.1016/0006-8993\(87\)91501-0](https://doi.org/10.1016/0006-8993(87)91501-0)
- 972 Siebold, C., Glonti, L., Glasauer, S., & Büttner, U. (1997). Rostral Fastigial Nucleus Activity in the Alert  
973 Monkey During Three-Dimensional Passive Head Movements. *Journal of Neurophysiology*,  
974 77(3), 1432–1446. <https://doi.org/10.1152/jn.1997.77.3.1432>
- 975 Stay, T. L., Laurens, J., Sillitoe, R. V., & Angelaki, D. E. (2019). Genetically eliminating Purkinje neuron  
976 GABAergic neurotransmission increases their response gain to vestibular motion. *Proceedings*  
977 *of the National Academy of Sciences*, 116(8), 3245–3250.
- 978 Sugihara, I., & Quy, P. N. (2007). Identification of aldolase C compartments in the mouse cerebellar  
979 cortex by olivocerebellar labeling. *The Journal of Comparative Neurology*, 500(6), 1076–1092.  
980 <https://doi.org/10.1002/cne.21219>
- 981 Turecek, J., & Regehr, W. G. (2020). *Synaptic inputs to the inferior olive from cerebellar and vestibular*  
982 *nuclei have distinct release kinetics and neurotransmitters* [Preprint]. Neuroscience.  
983 <https://doi.org/10.1101/2020.07.31.231290>
- 984 Valera, A. M., Binda, F., Pawlowski, S. A., Dupont, J.-L., Casella, J.-F., Rothstein, J. D., Poulain, B., &  
985 Isope, P. (2016). Stereotyped spatial patterns of functional synaptic connectivity in the  
986 cerebellar cortex. *ELife*, 5, e09862. <https://doi.org/10.7554/eLife.09862>



- 987 Vingerhoets, R. A. A., Medendorp, W. P., & Van Gisbergen, J. A. M. (2006). Time Course and Magnitude  
 988 of Illusory Translation Perception During Off-Vertical Axis Rotation. *Journal of*  
 989 *Neurophysiology*, *95*(3), 1571–1587. <https://doi.org/10.1152/jn.00613.2005>
- 990 Vingerhoets, R. A. A., Van Gisbergen, J. A. M., & Medendorp, W. P. (2007). Verticality Perception  
 991 During Off-Vertical Axis Rotation. *Journal of Neurophysiology*, *97*(5), 3256–3268.  
 992 <https://doi.org/10.1152/jn.01333.2006>
- 993 Voogd, J., Gerrits, N. M., & Ruigrok, T. J. H. (1996). Organization of the Vestibulocerebellum. *Annals of*  
 994 *the New York Academy of Sciences*, *781*(1 Lipids and Sy), 553–579.  
 995 <https://doi.org/10.1111/j.1749-6632.1996.tb15728.x>
- 996 Waespe, W., & Henn, V. (1979). The velocity response of vestibular nucleus neurons during vestibular,  
 997 visual, and combined angular acceleration. *Experimental Brain Research*, *37*(2).  
 998 <https://doi.org/10.1007/BF00237718>
- 999 Wearne, S., Raphan, T., & Cohen, B. (1998). Control of Spatial Orientation of the Angular  
 1000 Vestibuloocular Reflex by the Nodulus and Uvula. *Journal of Neurophysiology*, *79*(5), 2690–  
 1001 2715. <https://doi.org/10.1152/jn.1998.79.5.2690>
- 1002 Wolpert, D. M., Miall, R. C., & Kawato, M. (1998a). Internal models in the cerebellum. *Trends in*  
 1003 *Cognitive Sciences*, *2*(9), 338–347. [https://doi.org/10.1016/S1364-6613\(98\)01221-2](https://doi.org/10.1016/S1364-6613(98)01221-2)
- 1004 Wolpert, D. M., Miall, R. C., & Kawato, M. (1998b). Internal models in the cerebellum. *Trends in*  
 1005 *Cognitive Sciences*, *2*(9), 338–347. [https://doi.org/10.1016/S1364-6613\(98\)01221-2](https://doi.org/10.1016/S1364-6613(98)01221-2)
- 1006 Wylie, D. R., De Zeeuw, C. I., Digiorgi, P. L., & Simpson, J. I. (1994). Projections of individual purkinje  
 1007 cells of identified zones in the ventral nodulus to the vestibular and cerebellar nuclei in the  
 1008 rabbit. *The Journal of Comparative Neurology*, *349*(3), 448–463.  
 1009 <https://doi.org/10.1002/cne.903490309>
- 1010 Yakhnitsa, V., & Barmack, N. H. (2006). Antiphasic Purkinje cell responses in mouse uvula-nodulus are  
 1011 sensitive to static roll-tilt and topographically organized. *Neuroscience*, *143*(2), 615–626.  
 1012 <https://doi.org/10.1016/j.neuroscience.2006.08.006>
- 1013 Yakusheva, T. A., Blazquez, P. M., & Angelaki, D. E. (2008). Frequency-Selective Coding of Translation  
 1014 and Tilt in Macaque Cerebellar Nodulus and Uvula. *Journal of Neuroscience*, *28*(40), 9997–  
 1015 10009. <https://doi.org/10.1523/JNEUROSCI.2232-08.2008>
- 1016 Yakusheva, T. A., Blazquez, P. M., & Angelaki, D. E. (2010). Relationship between Complex and Simple  
 1017 Spike Activity in Macaque Caudal Vermis during Three-Dimensional Vestibular Stimulation.  
 1018 *Journal of Neuroscience*, *30*(24), 8111–8126. <https://doi.org/10.1523/JNEUROSCI.5779-09.2010>
- 1020 Yakusheva, T. A., Blazquez, P. M., Chen, A., & Angelaki, D. E. (2013). Spatiotemporal Properties of Optic  
 1021 Flow and Vestibular Tuning in the Cerebellar Nodulus and Uvula. *Journal of Neuroscience*,  
 1022 *33*(38), 15145–15160. <https://doi.org/10.1523/JNEUROSCI.2118-13.2013>
- 1023 Yakusheva, T. A., Shaikh, A. G., Green, A. M., Blazquez, P. M., Dickman, J. D., & Angelaki, D. E. (2007).  
 1024 Purkinje Cells in Posterior Cerebellar Vermis Encode Motion in an Inertial Reference Frame.  
 1025 *Neuron*, *54*(6), 973–985. <https://doi.org/10.1016/j.neuron.2007.06.003>
- 1026 Zhou, W., Tang, B. F., Newlands, S. D., & King, W. M. (2006). Responses of Monkey Vestibular-Only  
 1027 Neurons to Translation and Angular Rotation. *Journal of Neurophysiology*, *96*(6), 2915–2930.  
 1028 <https://doi.org/10.1152/jn.00013.2006>
- 1029 Zupan, L. H., Merfeld, D. M., & Darlot, C. (2002). Using sensory weighting to model the influence of  
 1030 canal, otolith and visual cues on spatial orientation and eye movements. *Biological*  
 1031 *Cybernetics*, *86*(3), 209–230. <https://doi.org/10.1007/s00422-001-0290-1>
- 1032